Journal of Molecular Spectroscopy 269 (2011) 211–225

Contents lists available at ScienceDirect

Journal of Molecular Spectroscopy

journal homepage: www.elsevier.com/locate/jms

A fitting program for molecules with two inequivalent methyl tops and a plane of symmetry at equilibrium: Application to new microwave and millimeter-wave measurements of methyl acetate

M. Tudorie [a,1], I. Kleiner [a,*], J.T. Hougen [b], S. Melandri [c], L.W. Sutikdja [d], W. Stahl [d]

[a] Laboratoire Interuniversitaire des Systèmes Atmosphériques (LISA), UMR 7583 CNRS/IPSL – Universités Paris-7 et -Est, 61 avenue du Général de Gaulle, 94010 Créteil Cedex, France
[b] Optical Technology Division, National Institute of Standards and Technology, Gaithersburg, MD 20899-8441, USA
[c] Dipartimento di Chimica "G. Ciamician", Università di Bologna, via F. Selmi 2, 40126 Bologna, Italy
[d] Institute of Physical Chemistry, RWTH Aachen University, Landoltweg 2, 52056 Aachen, Germany

ARTICLE INFO

Article history:
Received 7 May 2011
In revised form 12 June 2011
Available online 23 July 2011

Keywords:
G9 and G18 permutation–inversion groups
Internal rotation
Least squares fit program
Methyl acetate
Rotational transitions
Two inequivalent C3v tops

ABSTRACT

A program, called BELGI-Cs-2Tops, for fitting the high-resolution torsion–rotation spectra of molecules with two inequivalent methyl rotors and a plane of symmetry at equilibrium is described and applied to methyl acetate [CH_3—O—C(=O)—CH_3]. The G_{18} permutation–inversion group-theoretical considerations (allowed coordinate transformations, symmetry species for the basis set functions and various operators, etc.) used in the design of the program are presented, followed by a description of the structure of the program, which uses an "extreme" principal axis method and a two-step diagonalization procedure. Restriction to molecules belonging to the C_s point group at equilibrium allows the use of real arithmetic throughout the program. This program was used to carry out a weighted least-squares fit of more than 800 new microwave and millimeter-wave measurements on ground-state transitions in methyl acetate, leading to root-mean-square deviations of 4 kHz for the microwave lines and of 40 kHz for the millimeter-wave lines, i.e., to residuals essentially equal to the experimental measurement errors, and to heights for two internal rotation barriers of 102 cm^{-1} (acetyl CH_3) and 422 cm^{-1} (ester CH_3). Some of the difficulties in determining molecular parameters for a two-top molecule from a data set containing only torsional ground state information are discussed.

1. Introduction

The present paper consists of two parts. The first part describes a new program, called BELGI-Cs-2Tops, for fitting torsion–rotation spectra of molecules with: (i) two inequivalent methyl rotors, (ii) two different three-fold barriers, and (iii) a plane of symmetry at equilibrium. It thus represents another step in a planned series of papers aimed at providing the high-resolution spectroscopic community with a set of publically available programs that can be used to fit torsion–rotation levels for various types of molecules. The second part describes a fit using this program of extensive new microwave and millimeter-wave transitions in the ground (vibrational and torsional) state of methyl acetate. It can thus be considered as a first step toward preparing a methyl acetate atlas for astrophysical use.

At the present time only two of the planned series of programs are available on Z. Kisiel's PROSPE website [1]. The program BELGI-Cs [1,2] fits spectra of molecules with one methyl rotor, a three-fold barrier, and a plane of symmetry at equilibrium. The program BELGI-C_1 [1,3] fits spectra of molecules with one methyl rotor, a three-fold barrier, and no symmetry at equilibrium. A third program, designed to fit spectra of molecules with one methyl rotor, a six-fold barrier, and a plane of symmetry at equilibrium, has recently been used to treat microwave and millimeter-wave transitions in the (nearly free rotor) $m = 0$, 1, 2, and 3 states of toluene [4] and to treat the $0 \leqslant m \leqslant 6$ states of 1,1,1-trifluorotoluene [5].

There are already several programs in the literature capable of treating spectra of molecules with two inequivalent methyl rotors, which we very briefly review. (A somewhat longer discussion of their applications to one-top molecules is given in Ref. [6].)

The program XIAM [7] is designed specifically for internal-rotation problems involving up to three tops, and treats the internal rotation motion by determining eigenvalues and eigenvectors of a Hamiltonian containing appropriate kinetic energy operators and potential energy functions for the individual tops as well as a limited number of appropriate operators for the overall rotation

* Corresponding author. Fax: +33 1 4517 1564.
E-mail address: isabelle.kleiner@lisa.u-pec.fr (I. Kleiner).
[1] Present address: Université Libre de Bruxelles-Service de Chimie Quantique et Photophysique, Avenue F.D. Roosevelt, 50, C.P. 160/09, 1050 Bruxelles, Belgium.

0022-2852/$ - see front matter © 2011 Elsevier Inc. All rights reserved.
doi:10.1016/j.jms.2011.07.005

and for torsion–rotation interaction. It is quite user-friendly, but the results obtained using this program sometimes have observed-minus-calculated (obs − calc) values many times larger than the experimental measurement uncertainties [8], especially when the barrier is low.

The program ERHAM [9,10] is also designed specifically for internal-rotation problems, and treats the internal rotation motion by expanding torsional splittings and the behavior of various molecular constants as Fourier series depending mainly on the rotational quantum number K and the structural vector parameter $\boldsymbol{\rho}$. The strength of ERHAM is its ability to deal effortlessly and accurately with transitions at very high J (above 100). Since the Fourier expansions used give accurate results primarily for moderate to high torsional barriers, some fitting difficulties can be expected for molecules with low barriers, or for torsional levels that approach the top of a high barrier.

The very well-known and widely applicable program suite SPFIT/SPCAT [11] can also be used to fit two-top molecules, e.g., propane [12].

The program presented here is most closely related to that used only once in the literature [13], for a treatment of the microwave spectrum of the molecule N-methylacetamide [CH_3—NH—C(=O)—CH_3]. With this program, one iteration up to $J = 8$ used to take about 30 min on an Intel core i7 CPU 870, 2.93 GHz. In order to speed up the process we wrote a new code which uses a two step diagonalization procedure [14] similar to that in BELGI [2], and also uses a truncation in the number of basis functions retained after the first diagonalization step. The speeding up of the code was tested for two different procedures [15], either by using all subroutines (for diagonalization, inversion of the least-square matrix, timing) from the Math Kernel Library (MKL) [16] associated with the Intel Fortran compiler rather than from the Linear Algebra Package (LAPACK) subroutines [17], or by using the band matrix procedure and then using the corresponding LAPACK routines. We also increased the versatility of the code by adding more torsion–rotation interaction terms. One iteration now takes about 4 min up to $J = 10$ and 24 min up to $J = 19$ using the same PC mentioned above.

Methyl acetate is a molecule of astrophysical interest with two methyl tops which also happens to have a plane of symmetry in its equilibrium configuration. It therefore represents an excellent candidate for initial tests of the new program. However, up until this work the only published fit of microwave data for methyl acetate [18] made use of about 100 thirty-year-old measurements with $J \leqslant 5$ and $K_a \leqslant 3$, including some from an even earlier study of Williams, Owen, and Sheridan [19]. (It should be mentioned that Sheridan et al.'s analysis of the methyl acetate spectrum [18] was performed with a similar (though ancient) program using three different steps in the diagonalization.) We have undertaken a rather extensive methyl acetate measurement campaign for the present paper. More than 300 lines in the region from 8 to 40 GHz, with J values up to 8 and K_a values up to 3, were measured using the jet-cooled molecular-beam Fourier transform microwave spectrometer in Aachen, in either the 3–26.5 GHz mode [20] or the 26.5–40 GHz mode [21]. In addition, more than 500 lines in the region from 59.8 to 77.3 GHz, with J values up to 19 and K_a values up to 7, were measured using the Free Jet Absorption Millimeter Wave (FJAMMW) Stark-modulated millimeter-wave spectrometer in Bologna [22,23].

The rest of the paper is organized as follows. In Section 2 we review some necessary group-theoretical considerations. In Section 3 we discuss the structure of the program. In Sections 4 and 5 we discuss the available spectroscopic data set and our quantum chemistry calculations for methyl acetate. In Section 6 we apply the new program to methyl acetate. In Section 7 we give some discussion.

2. Symmetry considerations

The appropriate permutation–inversion (PI) group [24] for a two-inequivalent-methyl-rotor molecule with C_s point-group symmetry at equilibrium is G_{18}. (The assumption of C_s point-group symmetry and inequivalent methyl rotors requires the internal-rotation axes of both methyl tops to lie in the plane of symmetry at equilibrium.) If the hydrogen atoms of the two methyl rotors are numbered 1, 2, 3 and 4, 5, 6, respectively, and if all other atoms in the molecule are ignored, then the generators of G_{18} can be taken to be the PI operations (123), (456), and (23)(56)*. In fact, in a complete description of these PI operations, the permutation of all pairs of identical atoms lying symmetrically above and below the plane of symmetry (let us call them (*cd*) and (*ef*)) must be included, and this leads to generators of the form (123), (456), and (23)(56)(*cd*)(*ef*)*. We will nevertheless represent the last PI generator by a shorthand notation (23)(56)* in this paper and we use the character table for G_{18} given in terms of the generators (123), (456), and (23)(56)* in Table 1 of [13].

Fig. 1 gives the approximate structure for methyl acetate, together with atom numbering as described above.

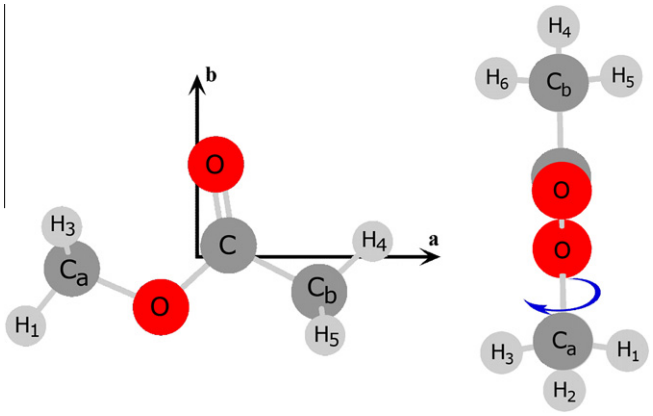

Fig. 1. The MP2/6-311++G** structure for methyl acetate. Left side: view from the positive c axis, with atom positions and labels corresponding to the structure defined in Eqs. (S1) and (S2) of the Supplementary Material with $\boldsymbol{R} = \boldsymbol{0}$ and $\chi = \theta = \phi = 0$ (so that the $\boldsymbol{R}_i$ give coordinates in the $z = a$, $x = b$, $y = c$ molecule-fixed axis system); with $z_{Ca}<0$ (so that the methyl group $C_aH_1H_2H_3$ is on the left); and with the internal rotation angles $\alpha_A = \alpha_B = 0$ (so that H_1 and H_4 lie in the xz plane). Note that out-of-plane atoms occur only in the two methyl tops. Right side: view from the positive b axis, with the methyl top at the bottom rotated by 120° in the direction of the arrow.

Table 1
Transformation properties of the rotational and torsional variables under the three generating operations of the PI group G_{18} for molecules with two inequivalent methyl tops and a plane of symmetry at equilibrium.

PI op.[a]	CM[b]	Rot. angles[c]	Torsional angles[d]	
E	$+\boldsymbol{R}$	χ, θ, ϕ	α_A	α_B
(123)	$+\boldsymbol{R}$	χ, θ, ϕ	$\alpha_A+2\pi/3$	α_B
(456)	$+\boldsymbol{R}$	χ, θ, ϕ	α_A	$\alpha_B+2\pi/3$
(23)(56)*	$-\boldsymbol{R}$	$\pi-\chi, \pi-\theta, \pi+\phi$	$-\alpha_A$	$-\alpha_B$

[a] Atom labels corresponding to these PI operations are defined in Fig. 1 and Section 2. The two tops are labeled A and B. The molecule-fixed variables in the other columns are defined in terms of the laboratory-fixed Cartesian coordinates of the atoms in Eq. (S2) of the Supplementary Material.

[b] Coordinates of the center of mass of the molecule in the laboratory-fixed Cartesian axis system.

[c] Rotational (Eulerian) angles for the molecule. The equivalent rotation [24] for the first three rows is the identity. For the last row it is $C_2(y)$.

[d] Torsional angles for methyl top A and B. Since the two tops are by hypothesis not symmetrically equivalent, there are no transformations where α_A is replaced by α_B.

Table 2
Symmetry species for torsional and rotational basis functions and for some operators in the torsion–rotation Hamiltonian.

Basis function[c]	Species[a]		Integers[b]		Basis function[d]	Species[a]		Integers[b]	
	G_{18}	G_9	σ_A	σ_B		G_{18}	G_9	σ_A	σ_B
$\cos(3k)\alpha_A$	A_1	A	0	0	$\|J, K_a = e, K_c = e\rangle$	A_1	A	0	0
$\sin(3k)\alpha_A$	A_2	A	0	0	$\|J, K_a = e, K_c = o\rangle$	A_2	A	0	0
$\exp(3k \pm 1)i\alpha_A$	E_1	$E_{1\pm}$	±1	0	$\|J, K_a = o, K_c = e\rangle$	A_1	A	0	0
$\cos(3k)\alpha_B$	A_1	A	0	0	$\|J, K_a = o, K_c = o\rangle$	A_2	A	0	0
$\sin(3k)\alpha_B$	A_2	A	0	0	Operator[e]				
$\exp(3k \pm 1)i\alpha_B$	E_2	$E_{2\pm}$	0	±1	J_x	A_2	A	0	0
Operator[f]					J_y	A_1	A	0	0
$P_{\alpha A}$	A_2	A	0	0	J_z	A_2	A	0	0
$P_{\alpha B}$	A_2	A	0	0					

[a] The character table for G_{18} is given in Table 1 of [13]. The character table for G_9 is given in Table 3 here. Symmetry species follow the notation of those tables.
[b] The symbols σ_A and σ_B represent a positive or negative integer, as defined in Table 3. Characters in G_9 for product functions can be calculated from these integers by simple addition, as in Eq. (2).
[c] Torsional basis functions for the two methyl rotors.
[d] Asymmetric-top rotational basis functions. The letters *e* and *o* represent even and odd, respectively.
[e] Molecule-fixed components of the total angular momentum.
[f] Momenta conjugate to the internal rotation angles of each top.

Following a slight variation of the procedures in Ref. [25], as described in detail in the Supplementary material (Text S1), we find that the three generators above lead to the intuitively expected transformations shown in Table 1 for the center of mass ***R***, rotational angles χ, θ, ϕ, and internal rotational angles α_A, and α_B. These transformations lead to the G_{18} symmetry species shown in Table 2 for the torsional and rotational basis set functions and for various operators occurring in the torsion–rotation Hamiltonian.

In the program, basis functions of species A_1 and A_2 are in fact put in the same block of the Hamiltonian. This corresponds essentially to using a smaller PI group G_9, formed from the two generators (123) and (456). The group G_9 has nine one-dimensional irreducible representations, with complex characters, as shown in Table 3. The symmetry species can be characterized by two integers σ_A and σ_B, where

$$(123)|\sigma_A, \sigma_B\rangle = \exp(2\pi i\sigma_A/3)|\sigma_A, \sigma_B\rangle$$
$$(456)|\sigma_A, \sigma_B\rangle = \exp(2\pi i\sigma_B/3)|\sigma_A, \sigma_B\rangle. \quad (1)$$

Values for these integers characterizing products of functions can be determined by simple addition, so that, for example,

$$|\sigma'_A, \sigma'_B\rangle|\sigma''_A, \sigma''_B\rangle = |\sigma_A = \sigma'_A + \sigma''_A, \sigma_B = \sigma'_B + \sigma''_B\rangle. \quad (2)$$

Table 3
Abbreviated[a] character table[b] for G_9.

Γ	E	(456)	(123)	(123) (456)	(123) (465)	σ_A[c], σ_B[c]	$C_3^A \times C_3^B$
A	$\varepsilon^0\varepsilon^0$	$\varepsilon^0\varepsilon^0$	$\varepsilon^0\varepsilon^0$	$\varepsilon^0\varepsilon^0$	$\varepsilon^0\varepsilon^0$	0, 0	AA
E_{1+}	$\varepsilon^0\varepsilon^0$	$\varepsilon^0\varepsilon^0$	$\varepsilon^{+1}\varepsilon^0$	$\varepsilon^{+1}\varepsilon^0$	$\varepsilon^{+1}\varepsilon^0$	+1, 0	EA
E_{1-}	$\varepsilon^0\varepsilon^0$	$\varepsilon^0\varepsilon^0$	$\varepsilon^{-1}\varepsilon^0$	$\varepsilon^{-1}\varepsilon^0$	$\varepsilon^{-1}\varepsilon^0$	−1, 0	EA
E_{2+}	$\varepsilon^0\varepsilon^0$	$\varepsilon^0\varepsilon^{+1}$	$\varepsilon^0\varepsilon^0$	$\varepsilon^0\varepsilon^{+1}$	$\varepsilon^0\varepsilon^{-1}$	0, +1	AE
E_{2-}	$\varepsilon^0\varepsilon^0$	$\varepsilon^0\varepsilon^{-1}$	$\varepsilon^0\varepsilon^0$	$\varepsilon^0\varepsilon^{-1}$	$\varepsilon^0\varepsilon^{+1}$	0, −1	AE
E_{3+}	$\varepsilon^0\varepsilon^0$	$\varepsilon^0\varepsilon^{-1}$	$\varepsilon^{+1}\varepsilon^0$	$\varepsilon^{+1}\varepsilon^{-1}$	$\varepsilon^{+1}\varepsilon^{+1}$	+1, −1	EE
E_{3-}	$\varepsilon^0\varepsilon^0$	$\varepsilon^0\varepsilon^{+1}$	$\varepsilon^{-1}\varepsilon^0$	$\varepsilon^{-1}\varepsilon^{+1}$	$\varepsilon^{-1}\varepsilon^{-1}$	−1, +1	EE
E_{4+}	$\varepsilon^0\varepsilon^0$	$\varepsilon^0\varepsilon^{+1}$	$\varepsilon^{+1}\varepsilon^0$	$\varepsilon^{+1}\varepsilon^{+1}$	$\varepsilon^{+1}\varepsilon^{-1}$	+1, +1	EE
E_{4-}	$\varepsilon^0\varepsilon^0$	$\varepsilon^0\varepsilon^{-1}$	$\varepsilon^{-1}\varepsilon^0$	$\varepsilon^{-1}\varepsilon^{-1}$	$\varepsilon^{-1}\varepsilon^{+1}$	−1, −1	EE

[a] The character for the inverse $P^{-1}$of any permutation operation P at the top of this table is the inverse of the character for P.
[b] Characters are given in the unusual form $\varepsilon^{\sigma A} \times \varepsilon^{\sigma B}$, where $\varepsilon^{\sigma} \equiv \exp(+2\pi\sigma i/3)$, to emphasize that transformation properties of each symmetry species Γ under (123) are determined only by σ_A, while transformation properties under (456) are determined only by σ_B. The values of σ_A and σ_B here correspond to those in the 9th and 10th columns of Table 1 of [13], respectively. Characters shown in that table for a given doubly degenerate species E_r of G_{18} can be obtained by adding the characters for E_{r+} and E_{r-} in this table.
[c] The exponents σ_A, $\sigma_B = 0$, 1, −1 in this table are defined so that $\sigma_i(\Gamma_p \times \Gamma_q) = \sigma_i(\Gamma_p) + \sigma_i(\Gamma_q)$ for any pair of species Γ_p and Γ_q and $i = A$ or B.

The Hamiltonian is then block-diagonalized into five submatrices characterized by $(\sigma_A, \sigma_B) = (0,0)$, $(1,0)$, $(0,1)$, $(+1,+1)$, and $(+1,-1)$, corresponding to the symmetry species A, E_{1+}, E_{2+}, E_{4+} and E_{3+}, respectively, in Table 3. The four submatrices with $(\sigma_A, \sigma_B) = (-1,0)$, $(0,-1)$, $(-1,-1)$, and $(-1,+1)$ are complex conjugates of those belonging to the separably degenerate species E_{1+}, E_{2+}, E_{4+} and E_{3+}, respectively, and have the same eigenvalues.

3. Description of the program

3.1. First diagonalization step

As pointed out in [14], there are advantages to solving the torsion–rotation Hamiltonian in two steps, where the first step deals with the torsion-*K*-rotation part of the problem, and the second step deals with all the rest. In the BELGI-Cs-2Tops program under discussion here we follow [14] by adopting a two-step diagonalization procedure, but we differ from [14] by using a modified principal-axis-method (PAM) [26], instead of the rho-axis-method (RAM) [27], which requires placing the *z* axis nearly parallel to "the" top axis. The PAM was chosen in the present program under the two assumptions that: (i) most molecules with two inequivalent CH_3 tops will be large enough that the ρ value for each top will be relatively small, and (ii) the PAM is well suited to problems with small ρ values [26]. The modification consists of transforming all contributions to the operator $(J_xJ_z + J_zJ_x)$ out of the two-top torsion–rotation Hamiltonian. (The analogous *xy* and *yz* terms vanish by symmetry in the C_s molecules considered here.) There are only two low order contributions to the $(J_xJ_z + J_zJ_x)$ terms. One comes from the moment of inertia of the atoms in the molecule, and is removed by going to the usual principal axis system. The second comes from cross terms in the PAM Hamiltonian [26] of the form $(F_A\rho_{Ax}\rho_{Az} + F_B\rho_{Bx}\rho_{Bz})(J_xJ_z + J_zJ_x)$, and is eliminated by a slight additional rotation about the *y* axis.

The basis set for our first (torsional) diagonalization step consists of products of exponentials of the form $(2\pi)^{-1}\exp(3k_A + \sigma_A)i\alpha_A \exp(3k_B + \sigma_B)i\alpha_B$ with the integers $|k_A|$ and $|k_B|$ both less than a basis set cutoff parameter *ktronc*. The Hamiltonian is diagonalized as separate blocks, each characterized by one of the five (σ_A, σ_B) pairs described at the end of Section 2.

Only the lowest order pure torsional operators of the Hamiltonian are considered in this first step, i.e.,

$$H_{tor} = \Sigma_{i=A,B}[F_iP_{\alpha i}^2 + (1/2)V_{3i}(1 - \cos 3\alpha_i)] + F_{AB}P_{\alpha A}P_{\alpha B} + V_{ABs}\sin 3\alpha_A \sin 3\alpha_B + V_{ABc}(1 - \cos 3\alpha_A)(1 - \cos 3\alpha_B). \quad (3)$$

(Note that in the computer program, and therefore also in Section 6, the letters *A* and *B* designating the two inequivalent tops are replaced by the Arabic integers 1 and 2, respectively.) In principle, higher order pure torsional operators could easily be moved into the first step, but it is hoped that the lowest order terms will take into account most of the top-top interaction. Normally, we set *ktronc* = 10, which means that 441 torsional basis functions are used in this first step. Following this diagonalization, we normally keep the lowest 42 = (2*ktronc*+1) × 2 torsional energy levels and wavefunctions for use in the second step. This corresponds (for similar torsional ladders in the two tops) to keeping somewhat more than the first six torsional levels for each top, together with all their combination levels.

Torsional matrix elements in the exponential basis set are well known [26] and will not be repeated here. Eigenfunctions and eigenvalues obtained from this first diagonalization step can be represented by $|v_A, v_B\rangle$ and $E(v_A, v_B)$. They do not depend in any way on the rotational quantum numbers.

3.2. Second diagonalization step

The full torsion–rotation Hamiltonian can be represented as

$$H = H_{tor} + H_{rot} + H_{tor-rot}, \quad (4)$$

where terms in this Hamiltonian can be constructed by taking symmetry-allowed and Hermitian products of a rotational factor (chosen from operators of the form $J_x^p J_y^q J_z^r$, where, *p*, *q*, and *r* are integer exponents) and a torsional factor for each top *i* = *A*, *B* (constructed in turn from products of operators of the form $P_{\alpha i}^p$, $\cos 3q\alpha_i$, $\sin 3r\alpha_i$, where *p*, *q* and *r* again represent integers). Since the two tops are by hypothesis inequivalent, torsional factors for each top are completely independent of each other in these operators (i.e., no top-top-interchange symmetrization is required).

Following the procedure in [13], we use a slightly modified PAM, in the sense that coefficients of the three quadratic rotational operators $(J_xJ_y + J_yJ_x)$, $(J_yJ_z + J_zJ_y)$, and $(J_zJ_x + J_xJ_z)$ are kept fixed to zero in the fits. Since there are contributions to these terms from some torsion–rotation terms, e.g., $+F_A\rho_{Ax}\rho_{Az}(J_zJ_x + J_xJ_z)$, this corresponds (implicitly) to using a contact transformation to remove these three terms completely, rather than to removing just the moment-of-inertia contributions to these terms. In addition, the coefficients of J_x^2, J_y^2, J_z^2 are simply labeled *B*, *C*, and *A*, respectively, so that the numerical values of these fitted "rotational constants" include some contributions not arising from the moment of inertia of the molecule.

Basis functions $|v_A, v_B\rangle\,|KJM\rangle$ for this second step consist of products of the lowest eigenfunctions from the first step diagonalization and the 2*J* + 1 symmetric top rotational functions for given *J*. Matrix elements of the rotational operators are well known. Our phase choice requires matrix elements of $J_x \pm iJ_y$ to be real and positive. Even though the torsional eigenfunctions from the first step can be represented conceptually as $|v_A, v_B\rangle$, such "local mode" labels can be both time-consuming to determine and misleading because of torsional state mixing. In practice, we therefore use only one index, *ivtor*, as a label for the eigenfunctions from the first diagonalization step, i.e., $|v_A, v_B\rangle$ is replaced by $|ivtor\rangle$, where *ivtor* just counts the eigenvalues in ascending order. Matrix elements of the torsional operators in the basis functions $|ivtor\rangle$ are computed from their expansions in the exponential basis set (as given by the eigenvectors from diagonalization step 1).

3.3. Banded-matrix diagonalization versus specific-processor-optimized non-banded diagonalization

Our initial fitting trials were performed using banded matrices similar to those described in Ref. [4], i.e., the basis-set quantum numbers *K*, v_A, and v_B were arranged in the array in such a way that all non-zero matrix elements appear within some diagonal band. Because it is uncommon to consider matrix elements with values of $|\Delta K|$ greater than some small even integer, the torsion–rotation matrix in this second diagonalization step can be put in banded form by letting *K* range from –*J* to +*J* in the outer do-loop (of our FORTRAN program) and then letting *ivtor* range from 1 to 42 in the inner loop. If matrix elements are limited to $|\Delta K| \leqslant 2$, this leads to a non-zero diagonal band with a half band width (counting the diagonal) of 3 × 42 = 126, for our normal operating conditions. In contrast, the full dimension *n* of the second diagonalization step matrix is approximately $n = (2J + 1)(42) \approx 84J$. As was done for toluene [4], we then used the DSBRDT routine from the Successive Band Reduction (SBR) package [28] to reduce the banded matrix to tridiagonal form and then used the corresponding LAPACK [17] routines to get eigenvalues and eigenvectors of the obtained tridiagonal matrix. This is in fact how the fit published here was obtained.

However during the course of our work we noted that for some of the processors specific-processor-optimized square-matrix diagonalization techniques can be competitive with the banded matrix routines cited above. It is advisable then to use the DSYEVR subroutine from the MKL library [16].

Finally, it also turned out that we can adjust either an energy cut-off or adjust how many eigenvalues and eigenvectors we actually want (e.g., we often set this number to the lowest 15(2*J*+1) eigenvalues) to further increase the speed of the calculation.

3.4. Checking procedures

In an attempt to remove as many errors from the code as possible, we have performed the following checks. First, we have reproduced to machine round-off a calculation for the A, E_1, E_2, E_3, E_4 energy levels up to *J* = 8 of the N-methyl acetamide molecule using Ohashi's program and the set of molecular constants from [13]. In addition, a number of tests were performed by comparing the calculations obtained by the new code with those obtained when using the one-top BELGI-C_s code. This comparison was done for each parameter found in both programs, i.e., the pure rotational parameters *A*, *B*, *C*, the centrifugal distorsion parameters Δ_J, Δ_{JK}, Δ_K, δ_J, δ_K, the torsional parameters $V_{3,1}$, $V_{3,2}$, F_1, F_2, and one higher order term $V_{3,1K}$ presently used in the fit (see Table 5 for definitions), and it allowed us to check energy levels for the A, E_1 and E_2 symmetry species. When we were doing these comparisons we set the Q_1 and Q_2 parameters in the BELGi-Cs-2Tops code to zero, and we set the ρ parameter in the one-top BELGI-Cs code to zero. This was necessary, because in the latter code, where the RAM method is followed, the first step diagonalization contains the rotation-torsion term $-2F\rho P_\alpha J_z$ [6,14] whereas in the BELGI-Cs-2Tops code, the equivalents of this term, $Q_1p_1J_z$ and $Q_2p_2J_z$, are dealt with in the second step. Therefore the two codes cannot be compared for these parameters.

4. The methyl acetate data set

An overview of the present data set is given in Table 4. The rotational quantum number and symmetry species coverage of the transitions in the fit is quite reasonable, but all transitions are within the ground torsional state of the molecule, i.e., there is no torsional excitation in either of the two methyl tops. For this reason, a number of important torsion–torsion interaction terms could not be unambiguously determined (see below). The maximum *J* value treated in this paper was chosen arbitrarily to be *J* = 19, which corresponds to an excitation energy in this degree

Table 4
Overview of the data set coverage[a] and fit quality.

I[d]	FTMW lines[b]				Mm-wave lines[c]			
	#[e]	rms[f]	J_{max}[g]	K_{max}[g]	#[e]	rms[f]	J_{max}[g]	K_{max}[g]
A	63	3.4	9	3	94	35	17	7
E_1	64	4.2	9	+3, −3	122	40	19	+7, −6
E_2	65	4.8	9	+3, −3	105	46	17	+6, −6
E_3	61	4.1	9	+3, −3	100	39	18	+6, −6
E_4	62	4.1	9	+3, −3	98	37	19	+7, −6

[a] Two lines from Ref. [18], at 25733.190 and 25786.250 MHz, were not remeasured. Their residuals are 26 and 13 kHz, respectively.
[b] These 315 Aachen measurements fit to their measurement error.
[c] These 519 Bologna measurements fit to their measurement error.
[d] Symmetry species of the lines in each row.
[e] Number of lines in each data group.
[f] Root-mean-square deviation of each data group in kHz.
[g] Largest J and K_a values in each data group (for E species the largest positive and negative K_a values are both given). Smallest J and K_a values are all 0, except for mm-wave lines which have $J_{min} = 3$.

of freedom of $(1/2)(B + C)J(J + 1) \approx 45\ cm^{-1}$ in methyl acetate. The maximum K value of $K_a = 6$ was determined by the available assigned transitions, and corresponds to an excitation energy in this degree of freedom of $[A - (1/2)(B + C)]K^2 \approx 8\ cm^{-1}$ in methyl acetate.

The symmetry species coverage is evenly distributed. There are six symmetry species in G_{18}, but the A_1 and A_2 species can be grouped together to give transitions within the species categories of A, E_1, E_2, E_3, and E_4. It can be seen from Table 4 that there are roughly equal numbers of microwave transitions (∼60) and roughly equal numbers of millimeter-wave transitions (∼100) for each of these five symmetry species. Since each asymmetric rotor transition $(J_{KaKc})' - (J_{KaKc})''$ splits into five tunneling components having exactly these symmetry species, we would expect in the ideal case to observe either zero or five components for each asymmetric rotor transition. In fact there are many cases where less than five components are included in the fit. Some cases of this type can be attributed to blending of the missing components, but other cases arise simply because the line search and assignment procedure was terminated after a finite length of time.

The data set contains a number of branches with five or six members (after which the branch typically goes out of the instrumental range), e.g., the A species R branch from $1_{11} - 0_{00}$ to $5_{15} - 4_{04}$ branch with three more members from $10_{1,10} - 9_{09}$ to $12_{1,12} - 11_{0,11}$, or the E_1, E_2, E_3, E_4 species Q branch from $6_{61} - 6_{52}$ to $17_{6,12} - 17_{5,13}$. The existence of such branches in the data set supports the assignments used in the fit more than a random collection of rotational transitions would. The lack of systematic drifts in the observed minus calculated values along

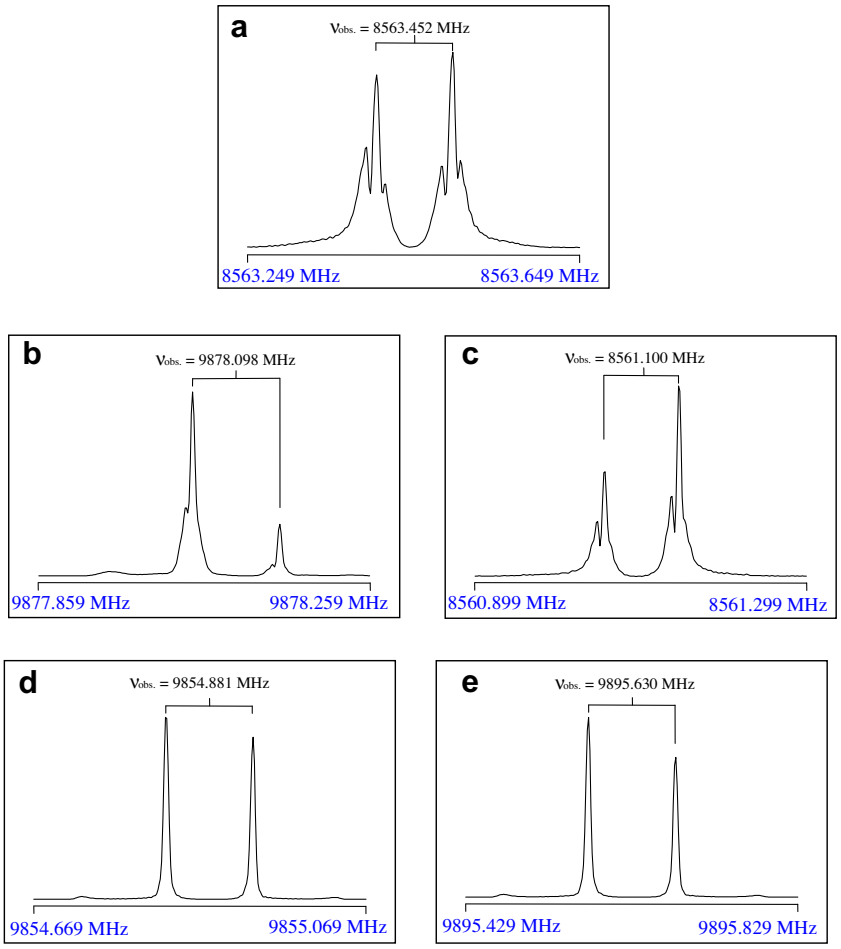

Fig. 2. Example of the tunneling components of the $J_{KaKc} = 2_{11} - 2_{02}$ asymmetric rotor transition measured with the FTMW spectrometer in Aachen. (a) The A tunneling component. Note the presence of rather broad partially resolved proton-spin hyperfine structure. (b) The E_1 tunneling component. Note the presence of somewhat less broad partially resolved proton-spin hyperfine structure. (c) The E_2 tunneling component, with partially resolved hyperfine structure resembling that in (b). (d) The E_3 tunneling component, with no apparent hyperfine broadening. (e) The E_4 tunneling component, again without any observable hyperfine structure, as in (d). These hyperfine patterns are characteristic of the symmetry species of the transition and persist at higher J and K.

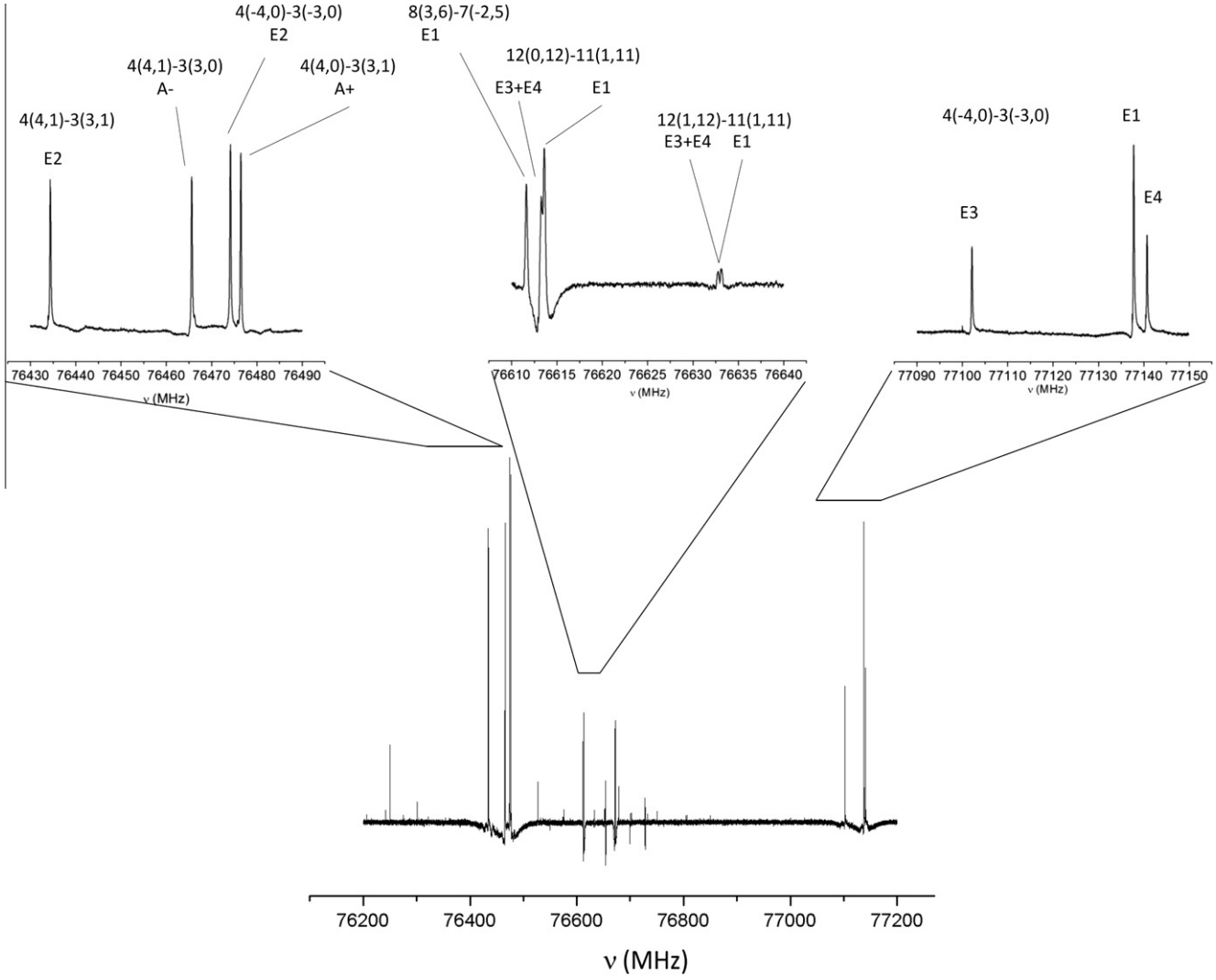

Fig. 3. Examples of transitions around 76 700 MHz, as measured with the millimeter-wave spectrometer in Bologna. The lower trace shows a 1 GHz overview scan, illustrating the density of lines and the large range of intensities in the spectrum. The upper traces show three regions with an approximately 10-fold expanded frequency scale. The left panel shows the four lines (using J_{KaKc} asymmetric rotor notation) $4_{41} - 3_{31}$ E_2, $4_{41} - 3_{30}$ A−, $4_{40} - 3_{30}$ E_2, and $4_{40} - 3_{31}$ A+ (see footnote of Table 6 for the definition of A+ and A-). The right panel shows the $4_{40} - 3_{30}$ lines of species E_3, E_1, and E_4. Note that these two panels contain transitions involving all five tunneling components of the 4_{40} upper state, which have relative statistical weights [13] of 2 (A, E_1, E_2) and 1 (E_3, E_4), respectively. Note further that the $4_{40} - 3_{30}$ E lines correspond to transitions between $-K$ levels, while the $4_{41} - 3_{31}$ E line is a transition between $+K$ levels in the signed K_a notation [27]. The center panel shows an $8_{36} - 7_{25}$ E_1 transition, which takes place between a $K'_a = +3$ and $K''_a = -2$ level, in signed K_a notation. The $12_{0,12} - 11_{1,11}$ transition is a triple blend, with the E_3, E_4, and E_1 components calculated to lie at 76613.177, 76613.332, and 76613.594 MHz, respectively. The $12_{1,12} - 11_{1,11}$ region contains an unresolved $E_3 \oplus E_4$ transition and an unblended E_1 transition calculated to lie at 76632.719 (E_3), 76632.801 (E_4), and 76633.131 (E_1) MHz, respectively. The relative intensities of the two observed $12_{1,12} - 11_{1,11}$ "lines" are equal, as expected from the relative statistical weights of 1 + 1 and 2.

such branches indicates the excellent quality of the quantum mechanical model used in the fit.

A measurement error of 4 kHz was assigned to the Fourier transform microwave lines, which are sometimes broadened by partially resolved hyperfine structure that presumably arises from the proton spins. Since these splittings were not treated theoretically, the ultimate measurement capability of the Aachen instrument (which is closer to 2 kHz) cannot be achieved for these lines. Fig. 2 shows five lines of different symmetry species measured in Aachen. Note that lines of E_3 and E_4 symmetry show no apparent proton-spin hyperfine structure. The qualitative hyperfine splitting patterns as a function of symmetry species illustrated in Fig. 2 were found empirically to persist in higher J and K transitions also, so they were used to help make symmetry species assignments during initial stages of the spectral analysis. A measurement error of 40 kHz was assigned to the millimeter-wave lines. Fig. 3 shows examples of lines measured in Bologna. Lines were weighted in the least squares fit (as usual) by $1/(\Delta\nu_{\mathrm{meas}})^2$, where $\Delta\nu_{\mathrm{meas}}$ is the assigned measurement error.

5. Quantum chemistry calculations

We do not determine an isotopic substitution structure in this work, but an excellent estimate for the geometry of methyl acetate can be obtained from *ab initio* techniques. Such a calculation was carried out at the MP2/6-311++G** level on the workstation cluster of the Center for Computing and Communication at the RWTH Aachen University using the commercial program package Gaussian 09 [29,30]. The rotational constants and the angle between the internal rotor and the *a* axis obtained from the *ab initio* calculation were used as starting values for assigning the spectra. These and other structural parameters are shown below to be in very good agreement with those obtained from our final spectral fit. The

absence of a calculated dipole moment component in the principal *c* axis direction confirms our assumption that the molecule has C_s symmetry and agrees with the experimental fact that no *c* type lines were observed in the spectrum. The atom coordinates from this *ab initio* calculation are deposited in the Supplementary Material (Table S1).

6. Fits of the methyl acetate data

6.1. Partial symmetry species fits

Table 2 of Ref. [13] shows the results of a separate least squares fit for transitions of each of the five G_{18} symmetry species (A, E_1, E_2, E_3, E_4) for N-methylacetamide. The purpose of such separate-species fits is: (i) to help assign transitions to the correct symmetry species and (ii) to help locate mismeasured lines, using a model with significantly fewer parameters than the complete model.

We could have followed Ref. [13] exactly, but because of the ready availability to us of a one-top BELGI program, we instead did the following. A-species fits and predictions were carried out from time to time at the beginning of the assignment process, using an ordinary Watson type Hamiltonian [31] with effective rotational constants, as is commonly done in all one-top internal rotation problems. For the present case of two inequivalent tops with a plane of symmetry at equilibrium, the absence of linear (and ultimately higher odd) powers of $\mathbf{J}$ in the effective rotational Hamiltonian for a $^tA_1$ torsional state that is well separated from $^tA_2$ torsional states follows from the fact that $P_{\alpha1}$ and $P_{\alpha2}$ are both of species A_2 in G_{18}, so that matrix elements of the form $\langle {}^t\Gamma|P_{\alpha1}|{}^tA_1\rangle$ and $\langle {}^t\Gamma|\ P_{\alpha2}|{}^tA_1\rangle$ vanish unless ${}^t\Gamma = {}^tA_2$. (Left superscripts *t*, *r*, or *tr* are used to indicate that the symmetries refer to pure torsional $J = K = 0$ or rotational or torsion-rotational states, respectively.)

Although we have not proved the following hypothesis by examining theoretically all of the higher-order contributions from top-top interactions, it seems reasonable to assume for a two-top problem with only weakly interacting tops, as we have also empirically verified earlier [32], that A and E_1 torsion–rotation species can be fit together using a one-top version of BELGI, and that A and E_2 species can also be fit together in the same way. Intuitively this rests on observing that in the symmetry notation using a pair of one-top local-mode species, we fit together the AA and EA states and then fit together the AA and AE states, under the assumption, for example, that in the A(A)and E(A) pair, internal rotation effects from the (A) state can be ignored, or at least can be taken into account by a one-top BELGI fit using effective constants. Such one-top fits were also carried out from time to time during the early assignment stage of this work.

Note that the procedure used here, unlike that in Ref. [13], does not allow separate symmetry-species fits of E_3 or E_4 species. Nevertheless, after we were confident of our A, E_1 and E_2 assignments, cycles of trial fits followed by predictions from our new two-top program seemed sufficient to make reliable E_3 and E_4 line assignments.

6.2. Full two-top fits

At this point we switched to fits using the two-top program described in Section 3. A very large number of exploratory fits were carried out, which led us finally to the following strategy for subsequent fits. The usual molecular rotational constants *A, B, C* and the associated five centrifugal distortion constants were fitted. This was possible because the data set covered a reasonably wide range of *J* and *K* values. The "internal rotation constants" F_1 (for top 1) and F_2 (for top 2) were initially fixed to values calculated from our *ab initio* equilibrium geometry, but the corresponding three-fold potential constants $V_{3,1}$ (for top 1) and $V_{3,2}$ (for top 2) were fitted. Finally we decided to fix F_2 to its value obtained in the partial fits done with BELGI one top. F_1 was fixed to its value obtained in a two-top fit with various higher order parameters held constant. The internal rotation constant F_{12}, (multiplying the top-top kinetic energy interaction operator $p_1p_2 \equiv P_{\alpha A}P_{\alpha B}$ in Section 2) was calculated [33] from the *ab initio* geometry, while the two top-top interaction constants of the next higher order in the potential energy (V_{12s} and V_{12c}) were fitted. Qualitatively speaking, these low order pure torsional kinetic and potential energy constants could not all be determined simultaneously because the present data set only contains information on the torsional ground state, and because one of the torsional barriers is rather high ($s = 4V_3/9F \approx 34$ for top 2). Fits based on the above treatment of selected low-order terms were then carried out after adding various trial combinations of higher-order terms.

Table 5 gives the 27 molecular constants varied in our final fit of 836 lines. This corresponds to about 31 lines per adjustable parameter, which the authors feel is quite satisfactory. Another way to judge the number of parameters in the fit is to note that we use ~5.4 parameters per symmetry species. This corresponds, in some sense, to using five or six parameters (e.g., *A*, *B*, *C*, two *D*'s, and a v_0) for each of five ordinary asymmetric rotor spectra with $0 \leqslant J \leqslant 19$ and $0 \leqslant K_a \leqslant 6$ coverage, which the authors again feel is quite satisfactory. The centrifugal distortion δ_K parameter was not found to be determined, and did not decrease the standard deviation so its

Table 5
Molecular parameters of methyl acetate obtained with the program BELGI-Cs-2Tops.

Operator[a]	Parameter[b]	Program[c]	Unit	Value[d]
J_z^2	A	OA	cm^{-1}	0.3818404(90)
J_x^2	B	B	cm^{-1}	0.1401459(17)
J_y^2	C	C	cm^{-1}	0.1025080(15)
$-\mathbf{J}^4$	Δ_J	DJ	cm^{-1}	0.000000023115(40)
$-\mathbf{J}^2J_z^2$	Δ_{JK}	DJK	cm^{-1}	−0.0000000321(21)
$-J_z^4$	Δ_K	DK	cm^{-1}	−0.000000602(68)
$-2\mathbf{J}^2\left(J_x^2-J_y^2\right)$	δ_J	$ODELN$	cm^{-1}	0.000000005973(17)
p_1^2	f_1	$F1$	cm^{-1}	5.554669[e]
p_2^2	f_2	$F2$	cm^{-1}	5.523464[e]
$p_1\ p_2$	f_{12}	$F12$	cm^{-1}	0.664[e]
$(1/2)(1-\cos3\alpha_1)$	$V_{3,1}$	$V31$	cm^{-1}	101.740(30)
$(1-\cos3\alpha_1)J_z^2$	$V_{3,1K}$	$V31K$	cm^{-1}	0.0021793(95)
$(1/2)(1-\cos3\alpha_2)$	$V_{3,2}$	$V32$	cm^{-1}	422.148(55)
$(1-\cos3\alpha_1)(1-\cos3\alpha_2)$	V_{12c}	$V12C$	cm^{-1}	−3.526(26)
$\sin3\alpha_1\sin3\alpha_2$	V_{12s}	$V12S$	cm^{-1}	34.24(28)
J_zp_1	q_1	$Q1$	cm^{-1}	−0.68129(12)
J_zp_2	q_2	$Q2$	cm^{-1}	−0.70434(10)
$J_z^3p_2$	q_{2K}	$Q2K$	cm^{-1}	−0.0000148(11)
J_xp_1	r_1	$R1$	cm^{-1}	−0.124446(42)
$\mathbf{J}^2J_xp_1$	r_{1J}	$R1J$	cm^{-1}	−0.0000002155(64)
J_xp_2	r_2	$R2$	cm^{-1}	−0.092967(28)
$(1/2)\left(J_z^2J_x+J_xJ_z^2\right)p_2$	r_{2K}	$R2K$	cm^{-1}	−0.00002098(35)
$J_zp_1p_2(p_1+p_2)$	q_{12p}	$Q12P$	cm^{-1}	−0.000212(11)
$J_xp_1p_2(p_1+p_2)$	r_{12p}	$R12P$	cm^{-1}	0.0001643(63)
$J_x^2p_1^2$	B_1	$B1$	cm^{-1}	0.000029552(79)
$J_x^2p_2^2$	B_2	$B2$	cm^{-1}	0.00001878(29)
$J_x^2p_1p_2$	B_{12}	$B12$	cm^{-1}	−0.00004979(61)
$J_y^2p_1^2$	C_1	$CC1$	cm^{-1}	0.000007308(31)
$J_y^2p_2^2$	C_2	$CC2$	cm^{-1}	0.00001760(26)
$J_y^2p_1p_2$	C_{12}	$CC12$	cm^{-1}	−0.00002424(40)

[a] Operator which the parameter multiplies in the program.
[b] Notation of Eq. (6) and Table 3 of Ref. [13], except for *A*, *B*, and *C*, where the prime was removed.
[c] Notation used in the program input and output.
[d] Value of the parameter obtained from the final least-squares fit, with one standard uncertainty (type A, $k = 1$ [34]) given in parentheses.
[e] These parameters were held fixed in the fit (see text).

Table 6
Observed[a] and calculated transition frequencies and residuals (all in MHz) for selected branches; symmetry species and upper and lower state energies (in cm^{-1}).

Upper state				Lower state				Observed (UNC)		Calculated	Obs − calc	Sym	E′	E″
J	K_A	K_C	P	J	K_A	K_C	P							
1	0	1	+	0	0	0	+	7253.536	(4)	7253.537	−0.001	A	100.1870	99.9450
2	0	2	+	1	0	1	+	14373.945	(4)	14373.945	0.000	A	100.6654	100.1870
4	0	4	+	3	0	3	+	27785.748	(4)	27785.745	0.003	A	102.3018	101.3749
5	0	5	+	4	0	4	+	34044.075	(4)	34044.073	0.003	A	103.4374	102.3018
10	0	10	+	9	0	9	+	64434.578	(40)	64434.585	−0.007	A	112.1536	110.0043
11	0	11	+	10	0	10	+	70563.797	(40)	70563.812	−0.015	A	114.5074	112.1536
1	1	1	+	0	0	0	+	13484.540	(4)	13484.533	0.007	A	100.3948	99.9450
2	1	2	+	1	0	1	+	19638.256	(4)	19638.254	0.002	A	100.8420	100.1870
3	1	3	+	2	0	2	+	25296.469	(4)	25296.468	0.002	A	101.5102	100.6664
4	1	4	+	3	0	3	+	30631.925	(4)	30631.921	0.005	A	102.3967	101.3749
5	1	5	+	4	0	4	+	35877.805	(4)	35877.802	0.004	A	103.4985	102.3018
10	1	10	+	9	0	9	+	64530.629	(40)	64530.597	0.032	A	112.1568	110.0043
11	1	11	+	10	0	10	+	70613.094	(40)	70613.069	0.025	A	114.5090	112.1536
12	1	12	+	11	0	11	+	76728.195	(40)	76728.221	−0.026	A	117.0067	114.5074
1	1	0	–	1	0	1	+	7330.719	(4)	7330.712	0.007	A	100.4315	100.1870
2	1	1	–	2	0	2	+	8563.452	(4)	8563.446	0.006	A	100.9521	100.6664
3	1	2	–	3	0	3	+	10644.001	(4)	10643.997	0.003	A	101.7300	101.3749
4	1	3	–	4	0	4	+	13772.629	(4)	13772.625	0.003	A	102.7612	102.3018
5	1	4	–	5	0	5	+	18051.570	(4)	18051.566	0.004	A	104.0395	103.4374
6	1	5	–	6	0	6	+	23387.025	(4)	23387.022	0.003	A	105.5562	104.7761
7	1	6	–	7	0	7	+	29494.840	(4)	29494.843	−0.003	A	107.3003	106.3165
8	1	7	–	8	0	8	+	36001.365	(4)	36001.370	−0.005	A	109.2597	108.0589
12	1	11	–	12	0	12	+	61321.883	(40)	61321.855	0.028	A	119.1114	117.0659
13	1	12	–	13	0	13	+	67255.406	(40)	67255.412	−0.006	A	122.0728	119.8294
14	1	13	–	14	0	14	+	73100.620	(40)	73100.625	−0.005	A	125.2364	122.7981
2	2	1	–	1	1	0	–	34297.623	(4)	34297.618	0.005	A	101.5755	100.4315
7	2	6	–	6	1	5	–	59991.500	(40)	59991.474	0.026	A	107.5573	105.5562
8	2	7	–	7	1	6	–	64177.430	(40)	64177.410	0.020	A	109.4410	107.3003
9	2	8	–	8	1	7	–	68492.242	(40)	68492.226	0.016	A	111.5444	109.2597
10	2	9	–	9	1	8	–	73124.289	(40)	73124.282	0.007	A	113.8636	111.4244
11	2	10	–	10	1	9	–	78151.578	(40)	78151.607	−0.029	A	116.3954	113.7885
2	2	0	+	1	1	1	+	35530.446	(4)	35530.444	0.002	A	101.5800	100.3948
5	2	3	+	4	1	4	+	66121.164	(40)	66121.133	0.031	A	104.6023	102.3967
2	2	1	–	2	1	2	+	21990.078	(4)	21990.077	0.001	A	101.5755	100.8420
3	2	2	–	3	1	3	+	23717.938	(4)	23717.933	0.005	A	102.3014	101.5102
5	2	4	–	5	1	5	+	28990.762	(4)	28990.757	0.005	A	104.4656	103.4985
6	2	5	–	6	1	6	+	32513.939	(4)	32513.937	0.002	A	105.8974	104.8129
7	2	6	–	7	1	7	+	36571.838	(4)	36571.841	−0.002	A	107.5573	106.3374
14	2	13	–	14	1	14	+	73332.883	(40)	73332.989	−0.106	A	125.2444	122.7983
2	2	0	+	2	1	1	–	18824.057	(4)	18824.049	0.009	A	101.5800	101.9521
3	2	1	+	3	1	2	–	17782.948	(4)	17782.947	0.002	A	102.3232	101.7300
4	2	2	+	4	1	3	–	17005.514	(4)	17005.513	0.001	A	103.3284	102.7612
5	2	3	+	5	1	4	–	16871.672	(4)	16871.671	0.002	A	104.6023	104.0395
6	2	4	+	6	1	5	–	17690.111	(4)	17690.110	0.001	A	106.1463	105.5562
7	2	5	+	7	1	6	–	19687.663	(4)	19687.660	0.002	A	107.9570	107.3003
8	2	6	+	8	1	7	–	23010.307	(4)	23010.307	0.000	A	110.0273	109.2597
9	2	7	+	9	1	8	–	27673.241	(4)	27673.245	−0.005	A	112.3475	111.4244
14	2	12	+	14	1	13	–	61079.352	(40)	61079.347	0.005	A	127.2738	125.2364
15	2	13	+	15	1	14	–	67654.016	(40)	67654.056	−0.040	A	130.8600	128.6033
1	0	1		0	0	0		7192.116	(4)	7192.116	0.000	E1	101.3346	101.0947
1	0	1		0	0	0		7253.486	(4)	7253.488	−0.001	E2	100.1970	99.9551
1	0	1		0	0	0		7192.834	(4)	7192.833	0.000	E3	101.3446	101.1047
1	0	1		0	0	0		7191.242	(4)	7191.241	0.001	E4	101.3448	101.1049
2	0	2		1	0	1		14280.027	(4)	14280.024	0.002	E1	101.8110	101.3346
2	0	2		1	0	1		14373.814	(4)	14373.813	0.000	E2	100.6765	100.1970
2	0	2		1	0	1		14280.948	(4)	14280.948	−0.001	E3	101.8210	101.3446
2	0	2		1	0	1		14278.781	(4)	14278.781	0.000	E4	101.8210	101.3448
4	0	4		3	0	3		27689.558	(4)	27689.559	0.000	E1	103.4398	102.5162
4	0	4		3	0	3		27785.302	(4)	27785.303	−0.001	E2	102.3118	101.3850
4	0	4		3	0	3		27689.807	(4)	27689.808	−0.001	E3	103.4498	102.5262
4	0	4		3	0	3		27688.456	(4)	27688.458	−0.002	E4	103.4498	102.5262
5	0	5		4	0	4		34043.478	(4)	34043.483	−0.005	E2	103.4474	102.3118
10	0	10		9	0	9		64376.602	(40)	64376.635	−0.033	E3	113.2861	111.1387
10	0	10		9	0	9		64376.602	(40)	64376.565	0.037	E4	113.2860	111.1386
10	0	10		9	0	9		64377.070	(40)	64377.055	0.015	E1	113.2761	111.1288
10	0	10		9	0	9		64434.086	(40)	64434.103	−0.017	E2	112.1635	110.0142
11	0	11		10	0	10		70510.391	(40)	70510.370	0.021	E1	115.6281	113.2761
11	0	11		10	0	10		70563.336	(40)	70563.367	−0.031	E2	114.5173	112.1635
11	0	11		10	0	10		70509.945	(40)	70509.957	−0.012	E3	115.6381	113.2861
11	0	11		10	0	10		70509.945	(40)	70509.937	0.008	E4	115.6379	113.2860
12	0	12		11	0	11		76652.469	(40)	76652.491	−0.022	E1	118.1850	115.6281
12	0	12		11	0	11		76652.078	(40)	76652.090	−0.012	E3	118.1949	115.6381
12	0	12		11	0	11		76652.078	(40)	76652.095	−0.017	E4	118.1948	115.6379

Table 6 (*continued*)

Upper state				Lower state				Observed (UNC)		Calculated	Obs − calc	Sym	E′	E″
J	K_A	K_C	P	J	K_A	K_C	P							
1	−1	0		0	0	0		16413.950	(4)	16413.949	0.001	E1	101.6423	101.0947
1	−1	0		0	0	0		16389.622	(4)	16389.620	0.002	E3	101.6514	101.1047
1	−1	0		0	0	0		16432.144	(4)	16432.144	0.000	E4	101.6530	101.1049
2	−1	1		1	0	1		24158.123	(4)	24158.125	−0.002	E1	102.1405	101.3346
2	−1	1		1	0	1		24135.829	(4)	24135.832	−0.003	E3	102.1497	101.3446
2	−1	1		1	0	1		24174.411	(4)	24174.412	−0.001	E4	102.1511	101.3448
6	−1	5		5	0	5		63437.543	(40)	63437.490	0.053	E1	106.6883	104.5722
6	−1	5		5	0	5		63439.406	(40)	63439.315	0.091	E4	106.6983	104.5822
7	−1	6		6	0	6		75370.430	(40)	75370.441	−0.011	E3	108.4320	105.9179
1	−1	0		1	0	1		7328.692	(4)	7328.686	0.006	E2	100.4415	100.1970
1	−1	0		1	0	1		9196.788	(4)	9196.787	0.001	E3	101.6514	101.3446
1	−1	0		1	0	1		9221.836	(4)	9221.833	0.003	E1	101.6423	101.3346
1	−1	0		1	0	1		9240.901	(4)	9240.903	−0.002	E4	101.6530	101.3448
2	−1	1		2	0	2		8561.100	(4)	8561.096	0.004	E2	100.9621	100.6765
2	−1	1		2	0	2		9854.881	(4)	9854.883	−0.002	E3	102.1497	101.8210
2	−1	1		2	0	2		9878.098	(4)	9878.101	−0.002	E1	102.1405	101.8110
2	−1	1		2	0	2		9895.630	(4)	9895.632	−0.002	E4	102.1511	101.8210
3	−1	2		3	0	3		11485.345	(4)	11485.348	−0.003	E3	102.9093	102.5262
3	−1	2		3	0	3		10641.587	(4)	10641.581	0.006	E2	101.7400	101.3850
3	−1	2		3	0	3		11504.491	(4)	11504.496	−0.005	E1	102.8999	102.5162
3	−1	2		3	0	3		11518.283	(4)	11518.284	−0.001	E4	102.9104	102.5262
4	−1	3		4	0	4		13770.225	(4)	13770.223	0.002	E2	102.7711	102.3118
4	−1	3		4	0	4		14287.395	(4)	14287.397	−0.002	E3	103.9264	103.4498
4	−1	3		4	0	4		14302.319	(4)	14302.323	−0.004	E1	103.9169	103.4398
4	−1	3		4	0	4		14312.055	(4)	14312.055	−0.001	E4	103.9272	103.4498
5	−1	4		5	0	5		18049.145	(4)	18049.139	0.006	E2	104.0494	103.4474
5	−1	4		5	0	5		18293.103	(4)	18293.105	−0.002	E3	105.1924	104.5822
5	−1	4		5	0	5		18304.387	(4)	18304.387	0.000	E1	105.1828	104.5722
5	−1	4		5	0	5		18310.403	(4)	18310.403	0.000	E4	105.1929	104.5822
6	−1	5		6	0	6		23394.067	(4)	23394.065	0.002	E1	106.6883	105.9079
6	−1	5		6	0	6		23384.367	(4)	23384.361	0.006	E2	105.5662	104.7861
6	−1	5		6	0	6		23385.473	(4)	23385.477	−0.004	E3	106.6980	105.9179
6	−1	5		6	0	6		23396.884	(4)	23396.885	−0.001	E4	106.6983	105.9178
7	−1	6		7	0	7		29282.677	(4)	29282.678	−0.001	E1	108.4223	107.4455
7	−1	6		7	0	7		29491.579	(4)	29491.573	0.006	E2	107.3102	106.3265
7	−1	6		7	0	7		29275.562	(4)	29275.567	−0.005	E3	108.4320	107.4555
7	−1	6		7	0	7		29282.838	(4)	29282.837	0.001	E4	108.4322	107.4554
8	−1	7		8	0	8		35586.264	(4)	35586.265	−0.001	E1	110.3725	109.1855
8	−1	7		8	0	8		35997.061	(4)	35997.063	−0.002	E2	109.2696	108.0688
8	−1	7		8	0	8		35579.491	(4)	35579.501	−0.010	E3	110.3823	109.1954
8	−1	7		8	0	8		35584.094	(4)	35584.096	−0.002	E4	110.3823	109.1953
12	−1	11		12	0	12		60182.664	(40)	60182.614	0.050	E1	120.1924	118.1850
12	−1	11		12	0	12		61311.672	(40)	61311.642	0.030	E2	119.1209	117.0758
12	−1	11		12	0	12		60172.672	(40)	60172.494	0.178	E3	120.2020	118.1949*
12	−1	11		12	0	12		60172.672	(40)	60172.698	−0.026	E4	120.2019	118.1948
13	−1	12		13	0	13		65971.070	(40)	65971.010	0.060	E1	123.1474	120.9469
13	−1	12		13	0	13		67243.844	(40)	67243.845	−0.001	E2	122.0823	119.8393
13	−1	12		13	0	13		65959.773	(40)	65959.762	0.011	E3	123.1570	120.9568
13	−1	12		13	0	13		65959.773	(40)	65959.677	0.096	E4	123.1568	120.9567
14	−1	13		14	0	14		71682.375	(40)	71682.305	0.070	E1	126.3050	123.9139
14	−1	13		14	0	14		73087.750	(40)	73087.790	−0.040	E2	125.2459	122.8079
14	−1	13		14	0	14		71669.930	(40)	71669.919	0.011	E3	126.3145	123.9238
15	−1	14		15	0	15		77344.750	(40)	77344.693	0.057	E1	129.6660	127.0861
1	1	1		0	0	0		11223.197	(4)	11223.200	−0.003	E1	101.4691	101.0947
1	1	1		0	0	0		13481.620	(4)	13481.617	0.002	E2	100.4048	99.9551
1	1	1		0	0	0		11200.997	(4)	11200.997	0.000	E4	101.4785	101.1049
1	1	1		0	0	0		11242.140	(4)	11242.143	−0.003	E3	101.4797	101.1047
2	1	2		1	0	1		18098.914	(4)	18098.919	−0.005	E1	101.9384	101.3346
2	1	2		1	0	1		19635.652	(4)	19635.653	−0.001	E2	100.8520	100.1970
2	1	2		1	0	1		18113.695	(4)	18113.700	−0.005	E3	101.9488	101.3446
2	1	2		1	0	1		18080.680	(4)	18080.682	−0.002	E4	101.9479	101.3448
3	1	3		2	0	2		25294.001	(4)	25294.003	−0.002	E2	101.5202	100.6765
3	1	3		2	0	2		24307.319	(4)	24307.322	−0.003	E4	102.6318	101.8210
3	1	3		2	0	2		24320.049	(4)	24320.052	−0.004	E1	102.6222	101.8110
3	1	3		2	0	2		24329.116	(4)	24329.121	−0.005	E3	102.6325	101.8210
4	1	4		3	0	3		29999.554	(4)	29999.557	−0.003	E1	103.5169	102.5162
4	1	4		3	0	3		30629.632	(4)	30629.633	−0.001	E2	102.4067	101.3850
4	1	4		3	0	3		30004.321	(4)	30004.325	−0.004	E3	103.5270	102.5262
4	1	4		3	0	3		29991.148	(4)	29991.152	−0.005	E4	103.5266	102.5262
5	1	5		4	0	4		35452.042	(4)	35452.045	−0.003	E1	104.6224	103.4398
5	1	5		4	0	4		35875.787	(4)	35875.791	−0.004	E2	103.5085	102.3118
5	1	5		4	0	4		35446.458	(4)	35446.462	−0.004	E4	104.6322	103.4498
5	1	5		4	0	4		35454.306	(4)	35454.312	−0.006	E3	104.6325	103.4498

(*continued on next page*)

Table 6 (*continued*)

Upper state				Lower state				Observed (UNC)		Calculated	Obs − calc	Sym	E′	E″
J	K_A	K_C	P	J	K_A	K_C	P							
10	1	10		9	0	9		64452.758	(40)	64452.698	0.060	E4	113.2885	111.1386
10	1	10		9	0	9		64453.105	(40)	64453.067	0.038	E3	113.2887	111.1387
10	1	10		9	0	9		64453.477	(40)	64453.444	0.033	E1	113.2787	111.1288
10	1	10		9	0	9		64529.996	(40)	64529.977	0.019	E2	112.1667	110.0142
11	1	11		10	0	10		70549.289	(40)	70549.267	0.022	E1	115.6294	113.2761
11	1	11		10	0	10		70612.547	(40)	70612.547	0.000	E2	114.5189	112.1635
11	1	11		10	0	10		70548.828	(40)	70548.869	−0.041	E3	115.6394	113.2861
11	1	11		10	0	10		70548.828	(40)	70548.701	0.127	E4	115.6392	113.2860*
12	1	12		11	0	11		76672.031	(40)	76672.028	0.003	E1	118.1856	115.6281
12	1	12		11	0	11		76727.711	(40)	76727.762	−0.051	E2	117.0766	114.5173
12	1	12		11	0	11		76671.602	(40)	76671.632	−0.030	E3	118.1956	115.6381
12	1	12		11	0	11		76671.602	(40)	76671.564	0.038	E4	118.1954	115.6379
6	6	0	+	6	5	1	−	74168.258	(40)	74168.229	0.029	A	113.1662	110.6923
7	6	1	+	7	5	2	−	74062.883	(40)	74062.873	0.010	A	114.8720	112.4015
8	6	2	+	8	5	3	−	73903.469	(40)	73903.453	0.016	A	116.8240	114.3589
9	6	3	+	9	5	4	−	73668.670	(40)	73668.663	0.007	A	119.0233	116.5660
10	6	4	+	10	5	5	−	73326.734	(40)	73326.714	0.020	A	121.4711	119.0252
11	6	5	+	11	5	6	−	72828.594	(40)	72828.577	0.017	A	124.1687	121.7394
12	6	6	+	12	5	7	−	72099.234	(40)	72099.212	0.022	A	127.1180	124.7130
13	6	7	+	13	5	8	−	71029.906	(40)	71029.901	0.005	A	130.3208	127.9515
14	6	8	+	14	5	9	−	69480.422	(40)	69480.397	0.025	A	133.7800	131.4623
15	6	9	+	15	5	10	−	67306.852	(40)	67306.815	0.037	A	137.4989	135.2538
6	6	1	−	6	5	2	+	74168.617	(40)	74168.629	−0.012	A	113.1662	110.6922
7	6	2	−	7	5	3	+	74065.250	(40)	74065.245	0.005	A	114.8720	112.4015
8	6	3	−	8	5	4	+	73913.539	(40)	73913.559	−0.020	A	116.8240	114.3585
9	6	4	−	9	5	5	+	73703.240	(40)	73703.243	−0.003	A	119.0233	116.5648
10	6	5	−	10	5	6	+	73427.437	(40)	73427.423	0.014	A	121.4710	119.0217
11	6	6	−	11	5	7	+	73086.961	(40)	73086.952	0.009	A	124.1684	121.7304
12	6	7	−	12	5	8	+	72696.000	(40)	72695.990	0.010	A	127.1168	124.6920
13	6	8	−	13	5	9	+	72287.906	(40)	72287.894	0.012	A	130.3178	127.9065
14	6	9	−	14	5	10	+	71919.742	(40)	71919.673	0.069	A	133.7726	131.3736
6	6	1		6	5	2		69737.273	(40)	69737.357	−0.084	E4	113.5843	111.2581
6	6	1		6	5	2		69772.281	(40)	69772.374	−0.093	E3	113.5920	111.2647
6	6	1		6	5	2		69778.336	(40)	69778.438	−0.102	E1	113.5807	111.2532
6	6	1		6	5	2		74126.500	(40)	74126.446	0.054	E2	113.1694	110.6969
7	6	2		7	5	3		69625.586	(40)	69625.663	−0.077	E4	115.2901	112.9677
7	6	2		7	5	3		69660.836	(40)	69660.922	−0.086	E3	115.2979	112.9742
7	6	2		7	5	3		69666.758	(40)	69666.869	−0.111	E1	115.2866	112.9627
8	6	3		8	5	4		69456.008	(40)	69456.065	−0.057	E4	117.2424	114.9256
8	6	3		8	5	4		69491.641	(40)	69491.702	−0.061	E3	117.2502	114.9322
8	6	3		8	5	4		69497.391	(40)	69497.477	−0.086	E1	117.2389	114.9207
8	6	3		8	5	4		73866.469	(40)	73866.440	0.029	E2	116.8272	114.3633
9	6	4		9	5	5		73645.109	(40)	73645.073	0.036	E2	119.0265	116.5700
9	6	4		9	5	5		69209.781	(40)	69209.798	−0.017	E4	119.4424	117.1338
9	6	4		9	5	5		69246.000	(40)	69246.002	−0.002	E3	119.4501	117.1403
9	6	4		9	5	5		69251.477	(40)	69251.529	−0.052	E1	119.4388	117.1288
10	6	5		10	5	6		68863.344	(40)	68863.379	−0.035	E4	121.8912	119.5942
10	6	5		10	5	6		68900.391	(40)	68900.422	−0.031	E3	121.8989	119.6006
10	6	5		10	5	6		68905.555	(40)	68905.592	−0.037	E1	121.8876	119.5892
10	6	5		10	5	6		73346.984	(40)	73346.950	0.034	E2	121.4743	119.0277
11	6	6		11	5	7		68429.766	(40)	68429.795	−0.029	E1	124.5868	122.3042
11	6	6		11	5	7		72982.414	(40)	72982.428	−0.014	E2	124.1718	121.7374
11	6	6		11	5	7		68425.133	(40)	68425.147	−0.014	E3	124.5980	122.3156
11	6	6		11	5	7		68386.820	(40)	68386.849	−0.029	E4	124.5904	122.3093
12	6	7		12	5	8		67786.789	(40)	67786.807	−0.018	E1	127.5380	125.2769
12	6	7		12	5	8		72584.570	(40)	72584.603	−0.033	E2	127.1207	124.6995
12	6	7		12	5	8		67782.969	(40)	67782.965	0.004	E3	127.5492	125.2882
12	6	7		12	5	8		67742.742	(40)	67742.731	0.011	E4	127.5416	125.2820
13	6	8		13	5	9		66937.047	(40)	66937.038	0.009	E1	130.7432	128.5104
13	6	8		13	5	9		72190.516	(40)	72190.579	−0.063	E2	130.3224	127.9143
13	6	8		13	5	9		66934.570	(40)	66934.554	0.016	E3	130.7543	128.5216
13	6	8		13	5	9		66891.148	(40)	66891.172	−0.024	E4	130.7469	128.5156
14	6	9		14	5	10		65865.047	(40)	65865.013	0.034	E1	134.2046	132.0076
14	6	9		14	5	10		71849.367	(40)	71849.453	−0.086	E2	133.7782	131.3815
14	6	9		14	5	10		65865.047	(40)	65865.042	0.005	E3	134.2157	132.0187
14	6	9		14	5	10		65816.289	(40)	65816.267	0.022	E4	134.2084	132.0130
15	6	10		15	5	11		64650.246	(40)	64650.218	0.028	E1	137.9249	135.7684
15	6	10		15	5	11		71625.859	(40)	71625.894	−0.035	E2	137.4887	135.0996
16	6	11		16	5	12		63576.113	(40)	63576.097	0.016	E1	141.9072	139.7865
16	6	11		16	5	12		71615.727	(40)	71615.731	−0.004	E2	141.4546	139.0658
16	6	11		16	5	12		63589.770	(40)	63589.696	0.074	E3	141.9181	139.7970
16	6	11		16	5	12		63516.125	(40)	63516.056	0.069	E4	141.9111	139.7924
17	6	12		17	5	13		63156.750	(40)	63156.691	0.059	E1	146.1545	144.0478
17	6	12		17	5	13		63088.457	(40)	63088.488	−0.031	E4	146.1585	144.0541*

Table 6 (*continued*)

Upper state				Lower state				Observed (UNC)		Calculated	Obs − calc	Sym	E′	E″
J	K_A	K_C	P	J	K_A	K_C	P							
18	6	13		18	5	14		63915.078	(40)	63915.016	0.062	E1	150.6688	148.5369
19	6	14		19	5	15		74022.562	(40)	74022.683	−0.121	E2	154.8810	152.4119*
6	−6	0		6	−5	1		73687.310	(40)	73687.253	0.057	E3	114.5044	112.0464
6	−6	0		6	−5	1		73720.360	(40)	73720.314	0.046	E4	114.5124	112.0533
6	−6	0		6	−5	1		73727.650	(40)	73727.623	0.027	E1	114.5011	112.0418
6	−6	0		6	−5	1		74160.770	(40)	74160.758	0.012	E2	113.1775	110.7038
7	−6	1		7	−5	2		73590.000	(40)	73589.932	0.068	E3	116.2069	113.7522
7	−6	1		7	−5	2		73623.150	(40)	73623.096	0.054	E4	116.2149	113.7591
7	−6	1		7	−5	2		73630.380	(40)	73630.354	0.026	E1	116.2036	113.7476
7	−6	1		7	−5	2		74056.469	(40)	74056.461	0.008	E2	114.8833	112.4130
8	−6	2		8	−5	3		73445.530	(40)	73445.489	0.041	E3	118.1551	115.7052
8	−6	2		8	−5	3		73478.870	(40)	73478.828	0.042	E4	118.1630	115.7120
8	−6	2		8	−5	3		73486.020	(40)	73486.006	0.014	E1	118.1518	115.7006
8	−6	2		8	−5	3		73900.891	(40)	73900.904	−0.013	E2	116.8353	114.3702
9	−6	3		9	−5	4		73280.141	(40)	73280.144	−0.003	E1	120.3466	117.9022
9	−6	3		9	−5	4		73239.492	(40)	73239.470	0.022	E3	120.3498	117.9068
9	−6	3		9	−5	4		73273.102	(40)	73273.082	0.020	E4	120.3578	117.9136
10	−6	4		10	−5	5		72995.125	(40)	72995.134	−0.009	E1	122.7891	120.3543
10	−6	4		10	−5	5		72954.227	(40)	72954.218	0.009	E3	122.7924	120.3589
10	−6	4		10	−5	5		72988.250	(40)	72988.238	0.012	E4	122.8003	120.3657
10	−6	4		10	−5	5		73357.406	(40)	73357.384	0.022	E2	121.4822	119.0353
11	−6	5		11	−5	6		72608.703	(40)	72608.716	−0.013	E1	125.4807	123.0587
11	−6	5		11	−5	6		72883.180	(40)	72883.147	0.033	E2	124.1797	121.7486
11	−6	5		11	−5	6		72567.461	(40)	72567.432	0.029	E3	125.4840	123.0634
11	−6	5		11	−5	6		72602.055	(40)	72602.052	0.003	E4	125.4918	123.0701
12	−6	6		12	−5	7		72090.891	(40)	72090.951	−0.060	E1	128.4227	126.0180
12	−6	6		12	−5	7		72160.490	(40)	72160.404	0.086	E2	127.1286	124.7216
12	−6	6		12	−5	7		72049.078	(40)	72049.102	−0.024	E3	128.4260	126.0227
12	−6	6		12	−5	7		72084.594	(40)	72084.626	−0.032	E4	128.4338	126.0294
13	−6	7		13	−5	8		71397.234	(40)	71397.275	−0.041	E1	131.6169	129.2354
13	−6	7		13	−5	8		71076.766	(40)	71076.662	0.104	E2	130.3307	127.9598
13	−6	7		13	−5	8		71354.500	(40)	71354.483	0.017	E3	131.6202	129.2401
13	−6	7		13	−5	8		71391.523	(40)	71391.499	0.024	E4	131.6280	129.2466
14	−6	8		14	−5	9		70453.203	(40)	70453.218	−0.015	E1	135.0651	132.7151
14	−6	8		14	−5	9		69499.680	(40)	69499.581	0.099	E2	133.7888	131.4706*
14	−6	8		14	−5	9		70408.602	(40)	70408.652	−0.050	E3	135.0685	132.7199
14	−6	8		14	−5	9		70448.445	(40)	70448.499	−0.054	E4	135.0762	132.7263
15	−6	9		15	−5	10		69127.234	(40)	69127.326	−0.092	E1	138.7696	136.4638
16	−6	10		16	−5	11		67210.602	(40)	67210.690	−0.088	E1	142.7332	140.4912
17	−6	11		17	−5	12		60904.582	(40)	60904.545	0.037	E2	145.7441	143.7125

[a] Estimated measurement uncertainties in kHz (type B, $k = 1$ [34]) are given in parentheses following the observed frequencies. Asymmetric rotor quantum numbers for upper and lower states are given on the left. For A species transitions a "parity" P is also given [27]. For E species transitions, K_a is signed [27]. Energies in cm^{-1} of the upper (E′) and lower (E″) states are given on the right.

value was fixed to zero. Table 6 gives observed minus calculated values for some low-K_a and some high-K_a transitions. It can be seen that almost all members (i.e., all J and all five symmetry species) of a given branch that fall in our microwave and millimeter-wave measurement ranges have been assigned and fitted. It can also be seen that the present program (and present computational power) gives a factor of 100 improvement in the E species residuals, when compared to the work of 30 years ago [18]. The full output from the fit, containing all fitted transitions, is deposited in the Supplementary material (Table S2).

The constants used in the fitting program are chosen [13] so that one constant multiplies only one operator, and vice versa. This makes understanding the least-squares correlation problems associated with these large fits less difficult, but it makes traditional physical interpretation of the constants more difficult, since some constants contain contributions from several physically different effects, some constants are the products of two physically meaningful parameters, etc. We thus convert [13] the fitting constants in Table 5 into constants that would occur in a more familiar PAM version [26] of the Hamiltonian, and present them in Table 7. Roughly speaking, constants in Table 5 down to q_1 have their usual meaning apart from corrections of a few percent [13]. The constants q_1 and r_1, as can be seen in Table 5 from the operators they multiply, are essentially $-2F_1\rho_{1a}$ and $-2F_1\rho_{1b}$ [26], respectively, with similar definitions for top 2. The constants below r_2 in Table 5 are higher-order torsion–rotation interaction terms that are represented by a variety of symbols in the literature.

It is easy to compare the experimental values in Table 7 with values determined from MP2/6-311++G** calculations with the Gaussian suite of programs [29,30]. The rotational constants A, B, C agree to better than 1%. The "rotational constants for internal rotation" F_1 and F_2 agree to about 5%, but it must be remembered that we fix these two parameters in our final two-top fit (to avoid divergence of the least-squares procedure) to values determined in our preliminary fits. These experimental values for F_1 and F_2 should thus not be taken too seriously until spectra have been analyzed involving torsionally excited states of both methyl tops. Values for the components of the vectors $\boldsymbol{\rho}_1$ and $\boldsymbol{\rho}_2$ along the a and b principal axes agree to within 3% for the larger component, but only to within 5% and 10% for the smaller component. Angles between the top axes and the principal axes agree to within a few degrees. All in all, we consider this agreement between various experimental and theoretical structure-based parameters to be completely satisfactory, indicating that *ab initio* values for these parameters make excellent starting values for least-squares fits in future applications of the present program.

Table 7
Two sets of molecular parameters for methyl acetate in the PAM system, one derived [13] from the least-squares fitted parameters in Table 5, the other from *ab initio* atom positions.

Parameter	Unit	BELGI-Cs-2Tops	G09[a]
A_{PAM}	MHz	10227.36(40)	10150.4
B_{PAM}	MHz	4164.544(55)	4189.5
C_{PAM}	MHz	3073.112(46)	3079.9
f_1	cm^{-1}	5.554669[b]	5.2752
$I_{\alpha 1}$	$uÅ^2$	3.21786(53)[c]	3.1956
$V_{3,1}$	cm^{-1}	101.740(30)	
	kJ/mol	1.2171(4)	
f_2	cm^{-1}	5.523464[b]	5.2407
$I_{\alpha 2}$	$uÅ^2$	3.18941(46)[c]	3.2167
$V_{3,2}$	cm^{-1}	422.148(55)	
	kJ/mol	5.0500(7)	
f_{12}	cm^{-1}	0.664[b]	0.6652[d]
ρ_{1a}		0.057353(11)[e]	0.05584
ρ_{1b}		0.0125581(38)[e]	−0.01306
ρ_1		0.058713(11)	0.05735
ρ_{2a}		0.0600130(93)[e]	0.05817
ρ_{2b}		0.0096735(26)[e]	−0.01160
ρ_2		0.0607877(92)	0.05932
θ	rad	−0.0316385(95)[f]	0.0369
$\angle(i_1,a)$	°	28.268(27)[g]	29.53
$\angle(i_1,b)$	°	61.732(11)[h]	60.47
$\angle(i_1,c)$	°	90.000	90.00
$\angle(i_2,a)$	°	21.596(31)[g]	25.79
$\angle(i_2,b)$	°	68.404(7)[h]	64.21
$\angle(i_2,c)$	°	90.000	90.00

[a] Parameters derived from the geometry obtained in a calculation at the MP2/6-311++G** level using Gaussian 09.
[b] Parameter held fixed in the fit, see Table 5.
[c] The internal rotation inertia moments $I_{\alpha 1}$ and $I_{\alpha 2}$ are derived from $I_{\alpha 1} = 505379.076/F_{01}$, where $F_{01} = AB/\left[\rho_{1a}^2 B^2 + \rho_{1b}^2 A^2\right]^{1/2}$ and similar equations for $I_{\alpha 2}$.
[d] See Eqs. (10), (13), and (14) of Ref. [13].
[e] Values derived from Eqs. (11) and (12) of Ref. [13].
[f] Angle about the y-axis, which relates the *a*, *b*, *c* PAM axes to the *x*, *y*, *z* axes.
[g] Angle between the methyl top axis and the PAM *a*-axis.
[h] Angle between the methyl top axis and the PAM *b*-axis: $\angle(i,b) = 90° - \angle(i,a)$.

7. Discussion

One way of gaining some pictorial understanding of the two-top energy levels of methyl acetate calculated from the constants in Table 5, together with some of the associated pure rotational transitions listed in Table 6, is by examining Fig. 4, which compares the splitting of the $J = 0$ energy levels with the splitting of the $10_{0,10} - 9_{0,9}$ transitions. The column labeled "$J = K = 0$ Levels" on the left of the overview in Fig. 4a shows the five tunneling components into which the 0_{00} rotational level is split, except that on the scale of this diagram, only the approximately 1.2 cm^{-1} splitting arising from torsional tunneling of the CH_3—C(=O) acetyl top through its "low" barrier of about 100 cm^{-1} is visible. The two levels are thus labeled A and E, as in any one-top internal rotation problem. The energy scale in cm^{-1} for this column begins at the bottom of the potential well, and is given on the left. The column labeled "$10_{0,10} - 9_{0,9}$ Transitions" on the right of Fig. 4a shows (in a vertical, rather than the usual horizontal display) the five observed components of the $10_{0,10} - 9_{0,9}$ transition, with frequency increasing downward and suitably scaled so that transitions of a given symmetry map onto $J = 0$ levels of that same symmetry. The frequency scale in MHz for this column is given on the right. Again on the scale of this diagram, only the approximately 57 MHz frequency splitting arising from internal rotation of the acetyl top can be seen, so that there are two transitions ($A \oplus E_2$) near 64435 MHz and three transitions ($E_1 \oplus E_3 \oplus E_4$) near 64377 MHz. The column labeled "$J = K = 0$ Levels" on the left of Fig. 4b displays the $J = 0$ energy levels again, but with an approximately 40-fold expansion in the energy scale. Now the approximately 0.01 cm^{-1} splitting caused by torsional tunneling in the CH_3—O ester top, with a much higher barrier of about 420 cm^{-1}, is visible, so the energy levels can be labeled in the usual two-top notation (AA, AE, etc.), which indicates the degeneracy in the

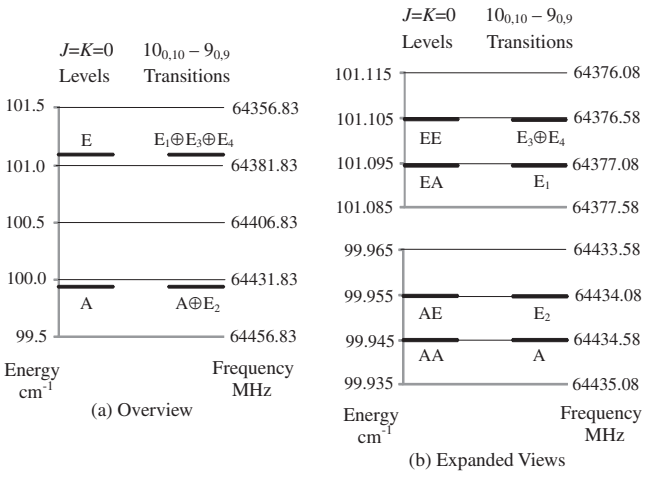

Fig. 4. Left side of overview (a): the $J = K = 0$ torsional levels in methyl acetate with energy increasing upwards (left scale). On the scale of this diagram we can see only the ~1.2 cm^{-1} splitting arising from torsional tunneling of the acetyl top CH_3—C(=O), with a barrier of 102 cm^{-1}. These two "one-top" levels are labeled A and E. Right side of overview (a): tunneling components of the $10_{0,10} - 9_{0,9}$ asymmetric-rotor transition, with frequency increasing downwards (right scale). Note that at this scale the splitting pattern for this transition is very similar to the splitting pattern for the $J = K = 0$ energy levels. Left side of expanded views (b): the $J = K = 0$ energy levels with the energy scale expanded ~40 times. The ~0.01 cm^{-1} splittings associated with tunneling of the CH_3—O ester top, with a torsional barrier of 422 cm^{-1}, are now visible, and the four resultant levels are labeled AA (non-degenerate), AE (doubly degenerate), EA (doubly degenerate), and EE (four-fold degenerate), to indicate their symmetry species with respect to each top. Right side of expanded views (b): tunneling components of the $10_{0,10} - 9_{0,9}$ transition, with energy increasing downwards. Apart from a change in sign, scale, and zero offset of the left and right axis labels in this figure, splittings of the components of this $K_a = 0 - 0$ asymmetric rotor transition are similar in all details to splittings of the components of the $J = K = 0$ energy pattern, including the lack of splitting of the $E_3 \oplus E_4$ transitions, which are in fact not experimentally resolved in the present study. This similarity [8,35] can be described for the $J' - J'' = 10_{0,10} - 9_{0,9}$ transition in methyl acetate by the empirical relation $\nu(\Gamma)_{transition}$ [MHz] = 69431.83 − 50 × $E(\Gamma)_{J=K=0}$ [cm^{-1}], where $\nu(\Gamma)_{transition}$ is the microwave transition frequency in MHz for symmetry species Γ = A, E_1, E_2, E_3, or E_4, and $E(\Gamma)_{J=K=0}$ is the energy in cm^{-1} for the $J = K = 0$ level of that symmetry.

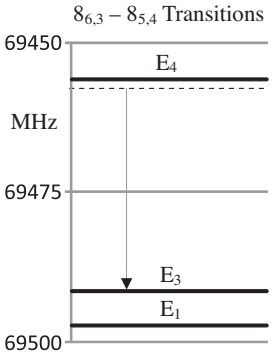

Fig. 5. Expanded view of the $EA = E_1$ and $EE = E_3 \oplus E_4$ components of the asymmetric rotor $8_{6,3} - 8_{5,4}$ tunneling splitting pattern. Because of Coriolis interactions between the internal rotation angular momentum of each top and the large $K_a = 5$ and 6 projections of the total angular momentum, the pattern of lines for this transition no longer resembles the $J = K = 0$ energy level diagram in Fig. 4b, as evidenced by the fact that the E_3 transition is now close to the E_1 transition, instead of being very close to the E_4 transition. The A and E_2 components of this transition are located at 73913.5 and 73866.4 MHz, respectively.

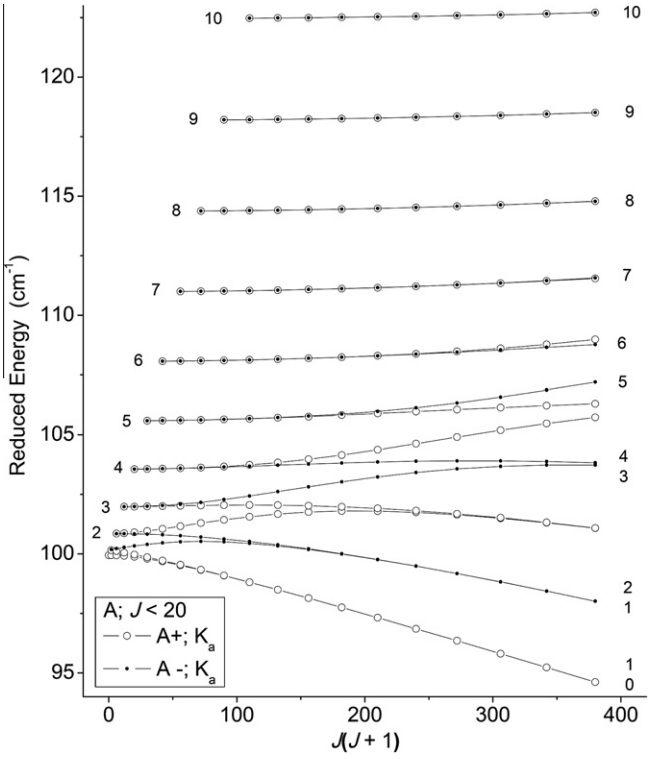

Fig. 6. Torsion–rotation (*tr*) energy level pattern for ^{tr}A states of methyl acetate in the ground torsional state of both rotors. Reduced energy values RE, obtained after subtraction of $(1/2)(B+C)J(J+1)$ from the real energies are plotted against $J(J+1)$, where the value of $(1/2)(B+C)$ is taken from Table 5. K_a quantum numbers for the series of A+ states (plotted as large open circles) are given on the left for $2 \leqslant K_a \leqslant 10$, and on the right for $K_a = 0$ and 1; K_a quantum numbers for the series of A- states (plotted as small dots) are given on the right. This reduced energy level diagram is very similar to that for a nearly rigid, near prolate asymmetric rotor with the *A*, *B*, and *C* values given in Table 5 (see text).

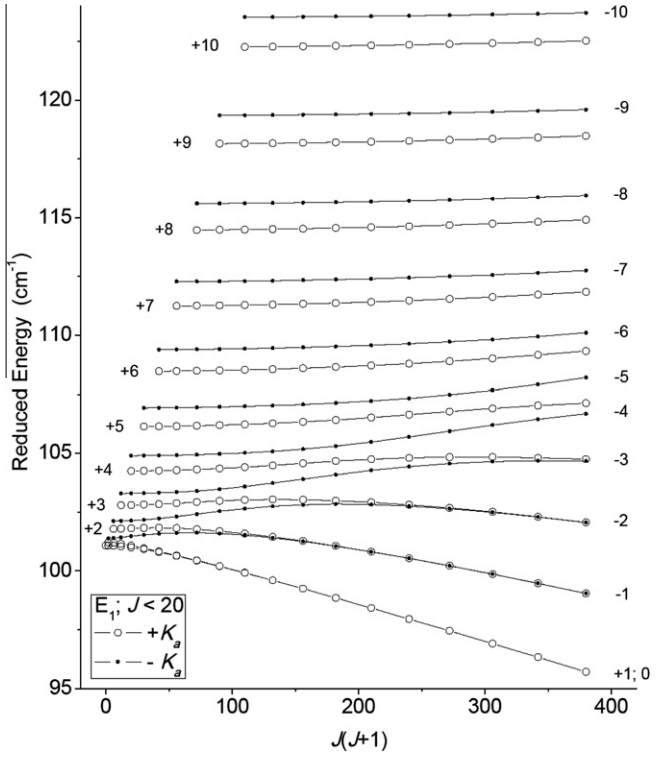

Fig. 7. Torsion–rotation energy level pattern for $^{tr}E_1$ states of methyl acetate in its torsional ground state, obtained by plotting the reduced energy RE as defined in Fig. 6. The $+K_a$ levels are plotted as large open circles, and their (positive) K_a values are given on the left (except for $K_a = 0$ and +1). The $-K_a$ levels are plotted as small dots, and their (negative) K_a values are given on the right. The $^{tr}E_1$ states correspond to EA states, so this diagram is very similar to that for a one-top molecule with the rotational constants *A*, *B*, *C*, and potential barrier $V_3 = V_{3,1}$ given in Table 5. The magnitude of the $+K_a$, $-K_a$ torsional splittings at high K_a is approximately proportional to K_a. At low K_a, these splittings are small compared to the rotational spacings, so the energy levels reorganize themselves into K_c clusters very similar to the K_c clusters in the lower right portion of Fig. 6.

torsional coordinate of top 1 (the acetyl top here) and top 2 (the ester top) associated with each wavefunction. Even on this expanded scale, however, the splitting of the EE levels caused by top-top interaction is not visible. The column labeled "$10_{0,10} - 9_{0,9}$ Transitions" in Fig. 4b shows the $10_{0,10} - 9_{0,9}$ transitions on this expanded scale. It can be seen that even in the finer details, the mapping of these transitions onto the $J = 0$ energy levels is rather exact. This phenomenon has been observed for other $K = 0$ tunneling splitting patterns [8,35], and an explanation for why it occurs has been proposed [35]. It can be used as an aid to $K = 0$ assignments in the early stages of spectroscopic analysis.

Fig. 5 shows the three tunneling components of the $8_{63} - 8_{54}$ Q branch pattern that arise from the EA and EE torsional states. It can be seen that the transition frequencies in this $K = 6 - 5$ pattern do not follow the $J = 0$ energy level pattern shown at the top of Fig. 4b, presumably because of the presence of significant torsion–rotation Coriolis effects for $K_a > 0$ that are absent in the pure torsional levels with $J = K_a = 0$, and almost absent in levels with $K_a = 0$.

Another way of gaining pictorial understanding is by examining Figs. 6–8, which plot reduced energy levels, i.e., Energy $-(1/2)(B+C)J(J+1)$, against $J(J+1)$ for states of A, E_1, and E_2 symmetry, respectively. For a rigid symmetric top, such plots would yield straight horizontal lines at the energies $[A - (1/2)(B+C)]K^2$. A rather extensive discussion of plots like these has been given for the one-top, six-fold-well problem in toluene [4], to which the reader is referred for background information. The situation for methyl acetate is not completely analogous to that for toluene, so we briefly discuss Figs. 6–8 now.

First-order interactions between the two torsional angular momenta and the total angular momentum vanish by symmetry for A states. Fig. 6 is thus essentially the same as for a nearly rigid asymmetric rotor. The main features of such a plot are well known: (i) horizontal straight lines for high K_a values, (ii) *K*-type doubling proportional to J^{2Ka} for low-*J*, low-K_a levels, and (iii) the development of tight K_c clusters for high-*J*, low-K_a levels.

E_1 wavefunctions essentially consist of the product of E wavefunctions for top 1 and A wavefunctions for top 2, so that first-order interaction between the torsional angular momentum and the total angular momentum vanishes for top 2, but is present for top 1. Fig. 7 is thus essentially the same as for the E states of a one-top asymmetric rotor. The main features of such a plot are somewhat less well known: (i) horizontal straight lines for high K_a values, but with the two lines for given $|K_a|$ displaced (when $|\rho_{1a}| \gg |\rho_{1b}|$) by $\pm 2F_1\rho_{1a}\langle p_1\rangle|K_a|$, where $\langle p_1\rangle$ is the expectation value for the torsional angular momentum in the torsional E state under consideration, (ii) a complicated region for low-*J*, low-K_a levels, where asymmetric-rotor *K*-type doubling effects and $\pm K_a$ torsional coupling effects compete, destroying the usefulness of both the $\pm K_a$ labeling scheme and the K_a, K_c labeling scheme, and (iii) the development of tight K_c clusters for high-*J*, low-K_a levels, where K_c returns as a useful label.

E_2 wavefunctions essentially consist of the product of A wavefunctions for top 1 and E wavefunctions for top 2, so that first-order interaction between the torsional angular momentum and the total angular momentum vanishes for top 1, but is present for top

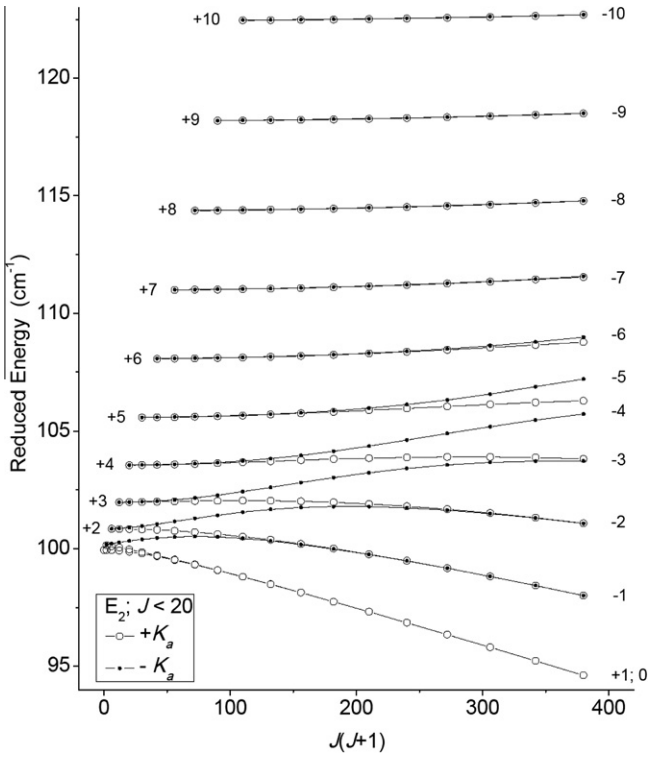

Fig. 8. Torsion–rotation energy level pattern for $^{tr}E_2$ states of methyl acetate in its torsional ground state, obtained by plotting the reduced energy RE as defined in Fig. 6. These levels correspond to AE states, where the high barrier of top 2 reduces almost to zero the expectation value of the torsional angular momentum that is symmetry allowed in the E state. For this reason, the energy levels on the scale of this figure look almost identical to those in Fig. 6 for the ^{tr}A (or AA) states.

2. Fig. 8 is thus again similar to that for the E states of a one-top asymmetric rotor, but for top 2 in methyl acetate the torsional splittings are much smaller than the asymmetric rotor splittings, and in fact cannot be seen on the scale of Fig. 8. As a result, Fig. 8 looks the same as Fig. 6 for the A states.

E_3 and E_4 wavefunctions consist of the product of E wavefunctions for both top 1 and top 2, so that first-order interaction between the torsional angular momentum and the total angular momentum is present for both tops. If the top axes are nearly parallel, as they are here, these two states can be thought of as representing the parallel and antiparallel combination of torsional angular momenta from top 1 and top 2. (Which state is parallel and which is antiparallel depends on a series of sign and phase conventions in the coordinate system.) Since splittings in top 2 are too small to be seen, reduced energy plots for E_3 and E_4 states look the same as Fig. 6 for E_1 states (see Figs. S1 and S2 in the supplementary material).

We now turn to an examination of the values of some of the molecular constants. It is interesting to note that the internal rotation barriers for the methyl group adjacent to the C=O bond are similar in methyl acetate and N-methylacetamide (102 cm^{-1} vs. 73 cm^{-1}), whereas the internal rotation barrier for the methyl group attached to the O atom is significantly higher than that for the methyl group attached to the NH group (422 cm^{-1} vs. 79 cm^{-1}).

The top-top interaction constant V_{12s}, which multiplies the $\sin3\alpha_1\sin3\alpha_2$ term, is about 34 cm^{-1}. This seems much too large to be a result of purely steric effects, and so we ascribe it to transfer of relative-orientation information from one top to the other through the bonds, rather than through space. The closely related constant V_{12c}, which multiplies $(1-\cos3\alpha_1)(1-\cos3\alpha_2)$, is ten times smaller, with a value of only -3.5 cm^{-1}. An intuitive understanding of the four main torsional potential terms can be obtained by expanding them as power series about the $\alpha_1 = \alpha_2 = 0$ equilibrium configuration, keeping only terms quadratic in the angles α_1 and α_2. We then obtain an expression of the form

$$(9/4)(V_{3,1}\alpha_1^2 + V_{3,2}\alpha_2^2) + 9V_{12s}\alpha_1\alpha_2, \quad (5)$$

which shows, for the small amplitude region of the two torsional motions, that $V_{3,1}$ and $V_{3,2}$ correspond essentially to different diagonal quadratic force constants for the torsional vibrations of the two inequivalent methyl tops, that V_{12c} does not contribute to any quadratic terms (its contributions begin at the quartic anharmonic level), and that V_{12s} corresponds to an off-diagonal quadratic force constant that couples the torsional modes of the two tops and tries to give the torsional normal modes some geared and antigeared character. In this sense, the term $\sin3\alpha_1\sin3\alpha_2$ distinguishes between in-phase ($\alpha_1\alpha_2 > 0$) and out-of-phase ($\alpha_1\alpha_2 < 0$) methyl-top oscillations when both tops are near their equilibrium configuration (small α_1 and α_2). It can be seen from Eq. (5) and Table 5 that the effects associated with this top–top torsional mode coupling near the equilibrium configuration are actually rather small in methyl acetate, since the difference $|V_{3,1} - V_{3,2}|$ is about 320 cm^{-1}, while V_{12s} is only about 34 cm^{-1}.

The kinetic energy term $F_{12}p_1p_2$ also distinguishes between in-phase and out-of-phase methyl-top oscillations. Because of the absence of information on excited torsional states, F_1, F_2, and F_{12} were constrained to values determined from the *ab initio* structural calculations. These indicate that F_{12} is about 12% of F_1 or F_2, showing that top-top torsional mode coupling arising from kinetic effects will also be relatively small in methyl acetate.

8. Conclusions

Application to methyl acetate of the new two-top program for molecules with a plane of symmetry shows that: (i) the program is capable of fitting modern spectral measurements to their experimental precision, and (ii) a fit with three iterations can be carried out up to $J = 15$ in less than one hour. This implies that the program is suitable for making line lists for astronomical purposes of any "weed molecules" with C_s point-group symmetry containing two threefold rotors. It should be noted, however, that it will in general be necessary to include in the fitted data set some transitions involving excited torsional levels of each top before predictions involving even short extrapolations in J or K in the ground torsional state will be reliable. In the authors' opinion, this requirement will be significantly more severe for two-top molecules than it is for one-top molecules, because the approximate doubling of torsional and torsion–rotational parameters in the two-top case makes it much more difficult to determine all necessary parameters from torsional ground state information alone.

This is particularly true for the present case of methyl acetate, where $V_{3,2} \gg V_{3,1}$. Since the higher barrier of top 2 in methyl acetate contributes much less to the observed spectral splittings than the lower barrier of top 1, the small contributions from $V_{3,2}$ and its higher-order correction terms are highly correlated with small changes in the much larger contributions from $V_{3,1}$ and its higher-order torsion–rotation correction terms, leading to systematic errors in the fitted constants caused by the spectroscopist's arbitrary choice of constants to be varied and constants to be kept fixed to zero in any given fit. This correlation should be broken, however, once data from excited torsional states (particularly of top 2) are included in the data set.

For further testing, the program is currently being applied to other molecules, in particular to three of the dimethylbenzaldeyde isomers [36], but the results are as yet very preliminary.

Acknowledgments

MT and IK acknowledge the financial support provided by ANR-08-BLAN-0054 during this work. LS and WS thank the Center for Computing and Communication of the RWTH Aachen University for free computer time and the Land Nordrhein-Westfalen for funds. They also want to thank Yelin Bao for her contribution during her research study in the Aachen workgroup. SM thanks the University of Bologna and MIUR (PRIN08, Project 356 KJX4SN_001) for financial support.

Appendix A. Supplementary material

Supplementary data for this article are available on ScienceDirect (www.sciencedirect.com) and as part of the Ohio State University Molecular Spectroscopy Archives (http://library.osu.edu/sites/msa/jmsa_hp.htm). Supplementary data associated with this article can be found, in the online version, at doi:10.1016/j.jms.2011.07.005.

References

[1] Z. Kisiel, Programs for ROtational SPEctroscopy. <http://www.ifpan.edu.pl/~kisiel/prospe.htm>.
[2] I. Kleiner, M. Godefroid, M. Herman, A.R.W. McKellar, J. Mol. Spectrosc. 142 (1990) 238–253.
[3] I. Kleiner, J.T. Hougen, J. Chem. Phys. 119 (2003) 5505–5509.
[4] V.V. Ilyushin, Z. Kisiel, L. Pszczółkowski, H. Mäder, J.T. Hougen, J. Mol. Spectrosc. 259 (2010) 26–38.
[5] V.V. Ilyushin, L.B. Favero, W. Caminati, J.-U. Grabow, ChemPhysChem 11 (2010) 2589–2593.
[6] I. Kleiner, J. Mol. Spectrosc. 260 (2010) 1–18.
[7] H. Hartwig, H. Dreizler, Z. Naturforsch. 51a (1996) 923–932.
[8] M. Schnell, J.T. Hougen, J.-U. Grabow, J. Mol. Spectrosc. 251 (2008) 38–55.
[9] P. Groner, J. Mol. Spectrosc. 156 (1992) 164–189.
[10] P. Groner, J. Chem. Phys. 107 (1997) 4483–4498.
[11] H.M. Pickett, J. Mol. Spectrosc. 148 (1991) 371–377. See also SPFIT/SPCAT package. <http://spec.jpl.nasa.gov>.
[12] B.J. Drouin, J.C. Pearson, A. Walters, V. Lattanzi, J. Mol. Spectrosc. 240 (2006) 227–237.
[13] N. Ohashi, J.T. Hougen, R.D. Suenram, F.J. Lovas, Y. Kawashima, M. Fujitake, J. Pyka, J. Mol. Spectrosc. 227 (2004) 28–42.
[14] E. Herbst, J.K. Messer, F.C. De Lucia, P. Helminger, J. Mol. Spectrosc. 108 (1984) 42–57.
[15] Vadim Ilyushin, private communication.
[16] Intel® Math Kernel Library. <http://software.intel.com/en-us/intel-mkl/>.
[17] LAPACK – Linear Algebra PACKage. <http://www.netlib.org/lapack/>.
[18] J. Sheridan, W. Bossert, A. Bauder, J. Mol. Spectrosc. 80 (1980) 1–11.
[19] G. Williams, N.L. Owen, J. Sheridan, Trans. Faraday Soc. 67 (1971) 922–949.
[20] U. Andresen, H. Dreizler, J.-U. Grabow, W. Stahl, Rev. Sci. Instrum. 61 (1990) 3694–3699.
[21] I. Merke, W. Stahl, H. Dreizler, Z. Naturforsch. 49a (1994) 490–496.
[22] S. Melandri, W. Caminati, L.B. Favero, A. Millemaggi, P.G. Favero, J. Mol. Struct. 352/353 (1995) 253–258.
[23] S. Melandri, G. Maccaferri, A. Maris, A. Millemaggi, W. Caminati, P.G. Favero, Chem. Phys. Lett. 261 (1996) 267–271.
[24] P.R. Bunker, P. Jensen, Molecular Symmetry and Spectroscopy, NRC Research Press, Ottawa, 1998.
[25] J.T. Hougen, J. Mol. Spectrosc. 256 (2009) 170–185.
[26] C.C. Lin, J.D. Swalen, Rev. Mod. Phys. 31 (1959) 841–892.
[27] J.T. Hougen, I. Kleiner, M. Godefroid, J. Mol. Spectrosc. 163 (1994) 559–586.
[28] C.H. Bischof, B. Lang, X.-.B. Sun, ACM Trans. Math. Software 26 (2000) 602–616.
[29] Gaussian 09, Revision A.1, M.J. Frisch, G.W. Trucks, H.B. Schlegel, G.E. Scuseria, M.A. Robb, J.R. Cheeseman, G. Scalmani, V. Barone, B. Mennucci, G.A. Petersson, H. Nakatsuji, M. Caricato, X. Li, H.P. Hratchian, A.F. Izmaylov, J. Bloino, G. Zheng, J.L. Sonnenberg, M. Hada, M. Ehara, K. Toyota, R. Fukuda, J. Hasegawa, M. Ishida, T. Nakajima, Y. Honda, O. Kitao, H. Nakai, T. Vreven, J.A. Montgomery, Jr., J.E. Peralta, F. Ogliaro, M. Bearpark, J.J. Heyd, E. Brothers, K.N. Kudin, V.N. Staroverov, R. Kobayashi, J. Normand, K. Raghavachari, A. Rendell, J.C. Burant, S.S. Iyengar, J. Tomasi, M. Cossi, N. Rega, J.M. Millam, M. Klene, J.E. Knox, J.B. Cross, V. Bakken, C. Adamo, J. Jaramillo, R. Gomperts, R.E. Stratmann, O. Yazyev, A.J. Austin, R. Cammi, C. Pomelli, J.W. Ochterski, R.L. Martin, K. Morokuma, V.G. Zakrzewski, G.A. Voth, P. Salvador, J.J. Dannenberg, S. Dapprich, A.D. Daniels, Ö. Farkas, J.B. Foresman, J.V. Ortiz, J. Cioslowski, D.J. Fox, Gaussian, Inc., Wallingford CT, 2009.
[30] Certain commercial products are identified in this paper in order to specify adequately the experimental or theoretical procedures. In no case does such identification imply recommendation or endorsement by the National Institute of Standards and Technology, nor does it imply that the products are necessarily the best available for the purpose.
[31] J.K.G. Watson, in: J.R. Durig (Ed.), Vibrational Spectra and Structure, vol. 6, Elsevier, Amsterdam, 1977, pp. 1–90.
[32] D.F. Plusquellic, I. Kleiner, J. Demaison, R.D. Suenram, R.J. Lavrich, F.J. Lovas, G.T. Fraser, V.V. Ilyushin, J. Chem. Phys. 125 (2006) 104312-1–104312-13.
[33] J.E. Wollrab, Rotational Spectra and Molecular Structure, Academic Press, New York, 1972.
[34] B.N. Taylor, C.E. Kuyatt, NIST Technical Note No. 1297, 1994. <http://www.nist.gov/pml/pubs/tn1297/index.cfm>.
[35] J.T. Hougen, N. Ohashi, J. Mol. Spectrosc. 159 (1993) 363–387.
[36] M. Tudorie, I. Kleiner, M. Jahn, J.-U. Grabow, M. Goubet, Poster L7 Poznan, 2010 (21st International Conference on HRMS).